Check for updates

APPLIED SCIENCES AND ENGINEERING

Emergent functional dynamics of link-bots

Kyungmin Son[1]†, Kimberly Bowal[2]†, Kwanwoo Kim[1], L. Mahadevan[2,3]*, Ho-Young Kim[1,4]*

Copyright © 2025 The Authors, some rights reserved; exclusive licensee American Association for the Advancement of Science. No claim to original U.S. Government Works. Distributed under a Creative Commons Attribution NonCommercial License 4.0 (CC BY-NC).

Synthetic active collectives, made of nonliving individuals that cooperatively change group shape and dynamics, hold promise for practical applications and understanding of their natural analogs. We investigate how simple steric interaction constraints between active individuals produce a versatile and functional system using the link-bot: a V-shape–based, single-stranded chain composed of active bots whose dynamics are defined by geometric linking constraints. A variety of emergent properties arises from this active polymer-like system, including locomotion, navigation, transportation, and competitive or cooperative interactions. By adjusting a few link parameters, we show how link-bots can perform diverse tasks, including traversing or obstructing narrow spaces, passing by or enclosing objects, and propelling loads in different directions. Overall, the reconfigurability of link-bots indicates their potential in developing programmable soft robotic systems with simple components and materials at any scale.

INTRODUCTION

Active collectives composed of many individuals can cooperatively execute functions that are impossible for solo individuals to accomplish, e.g., complex architectures, predation escape or prey capture, brood care in social insects, etc. Synthetic systems with these properties provide an opportunity to address functional applications or elucidate guiding principles in natural collectives. Designing these systems is challenging, and efforts can be categorized into two approaches: An intelligent group is created by complex individuals programmed to work together (*1*, *2*), or group intelligence is an emergent property that spontaneously arises from the interactions between simple agents (*3*). The former approach is represented by macroscale swarm robotics, in which individuals equipped with sensing, memory, computation, and/or communication capabilities can perform useful group behaviors, such as constructing a target shape or migrating toward a specific destination (*4*). However, this approach is naturally constrained by the limits on computation and communication at the individual level. These constraints are minimized in active particle systems that use the second approach through the use of a stimulus such as light (*5*–*7*), acoustics (*8*), or magnetic fields (*9*–*11*) to promote desired collective behaviors such as locomotion, flocking, navigation (*12*), and transportation (*13*). This is a useful approach, but it is limited by the requirement of an external global stimulus, which dictates the possible environment and materials as well as time and length scales.

A promising approach to circumventing these limitations involves generating collective behavior through physical interactions among active components, such as the flocking-like motion that emerges within granular shaken materials in the absence of any external control (*14*). Similar behaviors are seen in robot collectives through stochastic mechanical interactions that are adjusted at the group level through flexible and mobile boundaries (*15*–*17*) or through the type and strength of coupling between individuals (*18*–*20*). The latter method of connecting individuals into a flexible chain or loop shows promise at the microscale (*21*–*24*) and the macroscale (*25*, *26*). The ability to alter the morphology of a collective system has also been shown to allow complex behaviors (*27*, *28*) and adjustment to predetermined configurations (*29*) at any scale.

In this study, we investigate how simple steric interaction rules between active individuals produce a versatile active system with promising functionality by introducing the link-bot, a chain of forward-propelled bots defined by its internal geometric interaction constraints. In this active system, a few influential link parameters control the relative translation and rotation of each bot, allowing for breathing and flapping movements. These movements loosely control the link-bot shape and translate into predictable gaits when the link-bot encounters a boundary. When placed in complex environments, these morphological and translational movements produce a variety of emergent behaviors, including directed motion, interactions with obstacles, and load transport. The link-bot's versatility is demonstrated by its ability to perform multiple contrasting functions: maintaining or changing direction in obstructive terrains, infiltrating or blocking narrow spaces, maneuvering past or around objects, carrying objects forward or backward, and engaging in competitive or cooperative behaviors. Because of its scalability, material independence, and reconfigurability, this system paves the way for the development of functional, controllable, and autonomous collective systems using simple individuals at any scale.

RESULTS

Link-bot structure

Individual bots are three-dimensionally printed, consisting of a cylindrical body (diameter, $d = 1.5$ cm) on seven circumferentially equidistant legs, pictured in Fig. 1A(i). The legs are tilted, allowing the bot to self-propel in a preferred direction when placed on a vibrating surface. A circular flat arena with a diameter of 45 cm is vertically vibrated at a frequency of ≈80 Hz and an amplitude of 70 μm, causing a single bot to move at an average speed of 8 cm/s. The arena vibration properties are kept constant in all experiments. Figure 1A shows an example trajectory (ii) and speed profile (iii) of a single bot moving freely for 20 s. The corresponding log-log plot of the translational mean squared displacement with respect to time lag is given in Fig. 1A(iv), which shows ballistic motion ($\sim t^2$) over short timescales and diffusive motion ($\sim t$) over large timescales, typical of active Brownian motion.

[1]Department of Mechanical Engineering, Seoul National University, Seoul 08826, Korea. [2]School of Engineering and Applied Sciences, Harvard University, Cambridge, MA 02138, USA. [3]Departments of Physics, and Organismic and Evolutionary Biology, Harvard University, Cambridge, MA 02138, USA. [4]Institute of Advanced Machines and Design, Seoul National University, Seoul 08826, Korea.
*Corresponding author. Email: lmahadev@g.harvard.edu (L.M.); hyk@snu.ac.kr (H.-Y.K.)
†These authors contributed equally to this paper.

Downloaded from https://www.science.org at Seoul National University Library on May 11, 2025

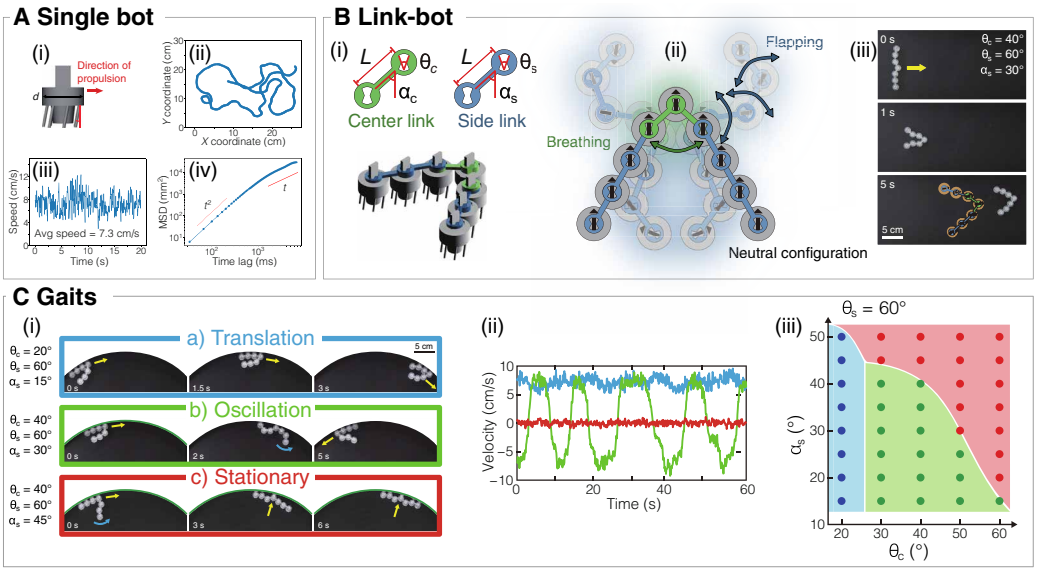

Fig. 1. The structure and dynamics of a single bot and link-bot in experiments. (**A**) A single bot consists of (i) a cylindrical body on tilted legs and topped with a crest. The (ii) trajectory, (iii) speed profile, and (iv) log-log diffusion plot of a single bot show characteristic active Brownian motion. MSD, mean squared displacement. (**B**) To construct a link-bot, rigid links connect *N* bots together in a symmetric V-shape. The links have (i) length *L*, notch angle θ, and spread angle α, with two center links connecting the center bot at the V vertex and side links connecting all other bots that make up the side chains. In the neutral V-shape configuration (ii), all bot crests are aligned in the direction of motion. The link constraints allow two main modes of link-bot movement: breathing (shown by the green arrow) in which the central V angle opens and closes and flapping (blue arrows) where the side chains bend inward and outward. (iii) Regardless of the initial configuration, the self-propelled link-bot relaxes into its neutral configuration (seen in the inset schematic) determined by the link properties. (**C**) (i) Link-bots exhibit three gaits at a boundary, controlled by the link angles: translation (unidirectional motion; shown in blue), oscillation (changing directions by flipping along the wall; shown in green), and stationary (pushing against the wall without substantial movement; shown in red). (ii) The changes in velocity for the three gaits. (iii) Phase diagram showing how the gaits change based on θ_c and α_s.

Bringing multiple bristle-bots into a collective provides rich and interesting behavior (*3*, *30*). Previous work on bristle-bots that are connected to form an active chain focuses on elastoactive systems (*20*, *31*, *32*) and the mechanical coupling of connected active chains (*24*, *32*, *33*). In this work, we focus on systems of bots that are connected by rigid links with rotational constraints: link-bots. The link-bot is created by connecting N bots with $N-1$ links in a V-shaped arrangement, inspired by the formations observed in troops and migrating birds (*34*). An example where $N=7$ is pictured in Fig. 1B. Each bot has a cuboidal crest on its top surface, which allows it to fit into the ribbon-shaped notches on both ends of the links. These links serve to maintain constant interbot distances between neighbors, transmit the motion of each bot to its neighbors, and constrain each bot's rotation. Links are characterized by three parameters: length between notches L, spread angle α, and notch angle θ. Spread angle α sets the geometric flexibility of the link-bot by prescribing the orientation of the links relative to bot orientations, causing the link-bot neutral configuration to be compact (low α) or spread out (high α). Notch angle θ sets the dynamic flexibility of the link-bot by allowing bots to move a lot (high θ) or very little (low θ) relative to their neighbors. Further details about the link angles and their effects on link-bot movement can be found in section S2 and fig. S2. The center bot and its neighbors are connected using two center links [pictured in green in Fig. 1B(i)], while all other bots are connected with side links (pictured in blue). The center and side links always have the same length $L=1.6$ cm, although their angles may differ and will be reported using subscripts c and s for the center and side, respectively. To produce a V-shaped arrangement, the links on one side of the center bot are reversed in relation to the links on the other side. This effectively suppresses undesired random deformations, such as crumpling and curling, which are often observed in active filaments (*35*). Two notable features of the link-bot in comparison to previous connected bristle-bot systems are the broken symmetry introduced by the V-shape and the threshold constraints imposed by the link notch angles. These features allow for a rich variety of collective behaviors to emerge from its characteristic active chain dynamics to provide a multifunctional soft robotic system.

Model

To complement our experiments, we developed a computational model to thoroughly evaluate the dynamical behaviors of the link-bot, explore the parameter space, and compare our predictions with observations. Each bristle-bot is modeled as an active Brownian particle, moving because of self-propulsion and diffusion. An example 20-s trajectory for a single simulated bot is shown in Fig. 2A(i), with a corresponding speed profile (ii) and diffusion plot (iii). The link-bot is simulated by adding translational and rotational constraints caused by the side and center links connecting the bots. Further details about the model are provided in the Methods section.

Locomotion

When not acted upon by outside forces, such as walls or obstacles, the link-bot moves forward in the direction of the center bot (i.e., the V vertex), generally maintaining a neutral configuration where all bots point in the same direction. The dimensions of this neutral configuration, examples of which are given in Figs. 1B and 2B, are controlled by the link-bot size, set by L and N, and the spread angle α.

Downloaded from https://www.science.org at Seoul National University Library on May 11, 2025

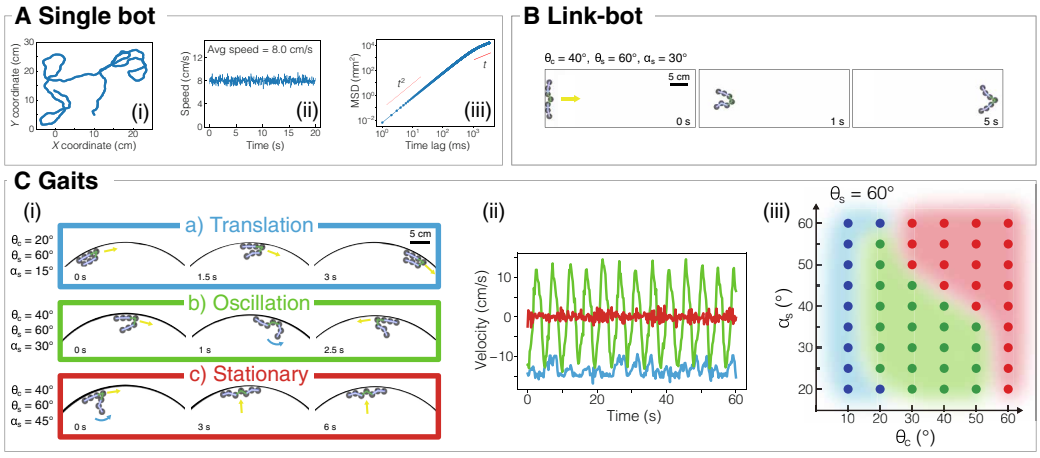

Fig. 2. Link-bot structure and dynamics in the computational model. (**A**) The (i) 20-s trajectory, (ii) speed, and (iii) log-log plot of mean squared displacement of a single bot are pictured, showing active Brownian motion matching that of the experiments. (**B**) Each self-propelled bot within a link-bot is modeled with translational and rotational constraints caused by the center and side links. This results in a noisy relaxation to the neutral configuration, where the bots form a V with all crests aligned, when the link-bot moves forward in space, regardless of the initial configuration. (**C**) (i) As in the experiments, the modeled link-bots exhibit three gaits at a wall: translation, oscillation, and stationary. (ii) The gaits are distinctive in their velocity patterns and (iii) show the same dependencies on θ_c and α_s at $\theta_s = 60°$ as seen in experiments.

The link-bot has two dynamic configuration modes due to the constraints imposed by the two link types: breathing and flapping. Breathing, shown by green arrows in Fig. 1B(ii), occurs when the central angle opens and closes between its minimum value, which is controlled by the steric interactions of the bots, and its maximum value of $\theta_c + 2\alpha_c$. The angle α_c is not independent and is determined by the dimensions of the link and the bot as $\alpha_c = \sin^{-1}\left[d/(2L)\right] + \theta_c/2$. This means that the range of breathing movements of the link-bot is controlled only by θ_c. Flapping, shown by blue arrows in Fig. 1B(ii), occurs when the side chains bend outward or inward. This flagella-like movement is known to be exhibited by active particle chains when they are pinned at one end (*31*, *32*, *36*). The asymmetry introduced by the V-shape of the link-bot allows this behavior to emerge without external pinning. The rotational notch angle θ_s and the side-chain spread angle α_s contribute in similar ways to the freedom of movement of a side bot. High values of θ_s and α_s allow for large flapping modes, producing floppy link-bot side chains that are able to bend substantially. In contrast, low values of these angles reduce flapping movement and produce rigid side chains that do not easily deform from the neutral configuration. These structural changes also translate into similar link-bot movement behaviors, which means that θ_s and α_s have the same phenotypic effects on the link-bot, as shown in fig. S7. Therefore, unless otherwise stated, in the following work, θ_s is kept at 60°, which provides a balance between the angle constraint and the freedom of bot motion. In this way, the side-link spread angle α_s controls the flexibility of the side chains and the resulting flapping movements. In conclusion, α_s and θ_c are the two critical parameters that control a link-bot's geometric neutral configuration and dynamic configuration mode, respectively.

To see how the link-bot's internal geometric parameters yield diverse behaviors, we investigate the link-bot's response upon encountering a wall. When the links do not impose any angular constraints on the bots, i.e., the link angles are set at 180°, the link-bot exhibits no directed motion or consistent interactions with the wall (shown in fig. S3 and movie S1). Simulations show that smaller link angles enhance the coordinated collective behavior of the link-bot. Figure 2C shows the behaviors of a link-bot consisting of $N = 7$ bots connected with different link angle values. The behavior can be categorized into three gaits: (i) unidirectional translation, (ii) oscillatory motion in which the link-bot periodically changes direction along the wall, and (iii) stationary. Figure 2C(ii) shows the velocity of the center bot as a function of time in each gait. The link-bot maintains a constant velocity when in translation, is periodic with a constant amplitude and frequency in the oscillation gait, and fluctuates around zero when stationary. The detailed dynamics of these gaits and how they can be understood by the torque applied around the center bot are discussed further in fig. S4 and section S4. A phase diagram showing the link-bot gaits at a wall as a function of θ_c and α_s is shown in Fig. 2C(iii). In line with the breathing and flapping modes, we see that the gait phenotypes are largely predicted by a small subset of the link-bot geometric parameters: the central angle θ_c and the side-chain flexibility α_s (detailed discussion found in the Supplementary Materials). The experimental observations of these gaits, shown in Fig. 1C and movie S1, agree well with those predicted by the model. The link-bot length, controlled by L, d, and N, are seen to have a weak effect on gait (figs. S5 and S6 and movie S2), which means that flexibility and θ_c are sufficient to predict gait (fig. S8).

Navigation

When put in complex environments, link-bots in experiments are able to navigate in distinct exploratory or exploitative ways, as seen in Fig. 3. These contradictory behaviors are products of the link-bot gait and its effect on wall interactions in each case and, thus, can be controlled by the link-bot angles. Exploratory behaviors, characterized by the link-bot traversing throughout its surroundings, occur when the link-bot is not substantially constrained by its interactions with a boundary. Examples of exploratory behavior shown in Fig. 3 are passing through a gap in a wall (Fig. 3A, top), traveling quickly through a channel (Fig. 3B), going around broken walls (Fig. 3C), and leaving a curved surface (Fig. 3D). Exploratory movement is generally favored by small to intermediate θ_c and α_s values that produce an oscillatory gait and keep bot self-propulsion tangential to

Downloaded from https://www.science.org at Seoul National University Library on May 11, 2025

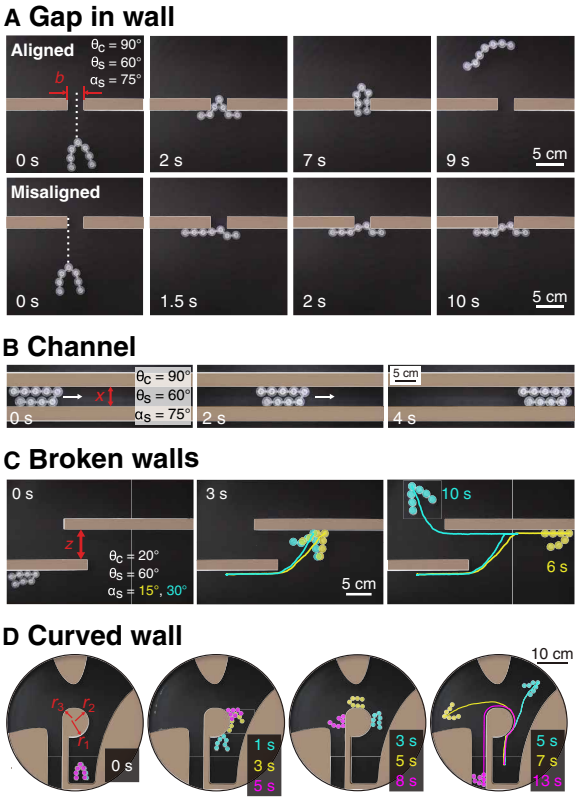

Fig. 3. Link-bots have programmable locomotion in a variety of environments. (**A**) The trajectories of two identical link-bots through a wall with a gap of $b = 3d$, showing that the alignment (top; with a white dotted line indicating the position of the center bot relative to the gap) or misalignment (bottom) of the center bot with the gap plays an important role in determining whether the link-bot will pass through or remain stuck at the wall. (**B**) A link-bot traveling along a narrow channel with width $x = 2d$. Additional experiments revealed that increasing the side-link spread angle α_s slows the link-bot's movement through the channel. (**C**) Upon encountering two walls with a spacing of $z = 4d$, link-bots with different side-link angles either pass through the maze of walls (blue) or remain trapped at a wall (yellow). (**D**) The link angles of a link-bot control the distance it will travel along a curved surface. An obstacle with three curvatures ($r_1 / d = 3.5, r_2 / d = 2.8, r_3 / d = 2$) can thus be used to sort link-bots of different properties. Shown here are link-bots with $\theta_c = 20°, \alpha_s = 15°$ (blue), $\theta_c = 40°, \alpha_s = 30°$ (yellow), and $\theta_c = 20°, \alpha_s = 45°$ with the left-most side link at 0-s inverted (magenta).

gaps, channel walls, and curved surfaces. In the example with discontinuous parallel walls (Fig. 3C), the exploratory link-bot, shaded in blue, navigates around the edges to continue past wall segments. This behavior is controlled by adjusting α_s to produce intermediate side-chain flexibility or changing θ_c to generate an oscillatory gait (for more details regarding the probabilities of these dynamics in the noisy system, see fig. S13). In an environment with curved boundaries, decreasing the link-bot flapping and breathing modes, through the use of lower α_s and θ_c values, causes the link-bot to leave the surface and explore its surroundings.

In contrast, localized exploitative behaviors, such as blocking a gap in a wall (Fig. 3A, bottom), traveling slowly through a channel (Fig. 3B), getting stuck at broken walls (Fig. 3C), or following a curved surface (Fig. 3D), dominate when the link-bot remains relatively stationary. Depending on the environment, this occurs at large or small values of the link angles. When rotational constraints are weak (i.e., θ_c or α_s are large), the resulting large breathing and flapping movements reach a stable state along straight surfaces where the bots are pushing against the walls so that normal or frictional forces restrict movement. In an environment with multiple walls, setting the link constraint angles to small values will produce an exploitative link-bot that does not pass through a maze of walls since it moves in the translation gait and is unable to change directions when encountering a new boundary (see the yellow link-bot in Fig. 3C). A link-bot with large link angles will have a stationary gait that causes it to remain fixed at a wall and therefore fail to progress through a maze. Similarly, when a link-bot enters a narrow channel, its movement is strongly constrained by the parallel surfaces. A high α_s value allows free rotation of bots toward both walls, increasing the active forces pointing into the walls and causing the link-bot speed to decrease (geometric prediction compared to experiments in fig. S11 and movie S4). This behavior is independent of link-bot length for $N = 7, 9$, and 11 (fig. S11C).

The position of the link-bot when encountering small boundary features can be an important factor for subsequent behaviors. For example, when the approaching center bot does not align with a gap in the wall, the link-bot sometimes will not bend inward, and the resulting high resistance from the narrow gap and the adjacent wall prevents its passage through the gap, causing highly exploitative behavior (Fig. 3A, bottom, and also shown in movie S3). To allow further control, an asymmetry can be added to the link-bot, such as the inversion of one of the end side links. This simple adjustment induces one-sided inward propulsion (fig. S14E), thereby enabling the link-bot to rotate around obstacles with substantial curvature without moving away from the surface (fig. S14F and movie S4). This expands the range of link-bot behaviors in this environment, allowing for an effective self-sorting mechanism such as that shown in Fig. 3D for three link-bots around one wall of varying curvatures.

These few barrier environments shown in Fig. 3 can be extended to an arbitrary number of walls for increasingly complex and realistic environments, such as a building layout or maze, through which link-bot behavior can be controlled using its internal geometric constraints. More details and examples are shown in figs. S9, S10, and S12 and movies S3 to S5.

Transportation and interactions

The link-bot model is a useful tool to further explore link-bot functionality in complex scenarios to predict and design link-bot behaviors. We present simulation results showing how link-bots balance directed motion and structural flexibility to interact with mobile objects in useful ways.

Adjusting the geometric properties of the link-bot produces many different transportation behaviors, some of which are shown in Fig. 4. Here, the center link angle is kept at $\theta_c = 90°$, so the breathing movement is minimally constrained. This allows the behavior to be controlled by α_s and N only, although it should be noted that low values of θ_c will reduce the allowed breathing mode angle and cause the same effect as low α_s values by reducing the link-bot contact with the object. When the link-bot is relatively short and the object is large, the link-bot carries the object forward. As the link-bot length increases, it is more likely to move around and away from the object. Link-bots interacting with relatively small objects are likely to carry the object backward. At some intermediate values, the link-bot

Downloaded from https://www.science.org at Seoul National University Library on May 11, 2025

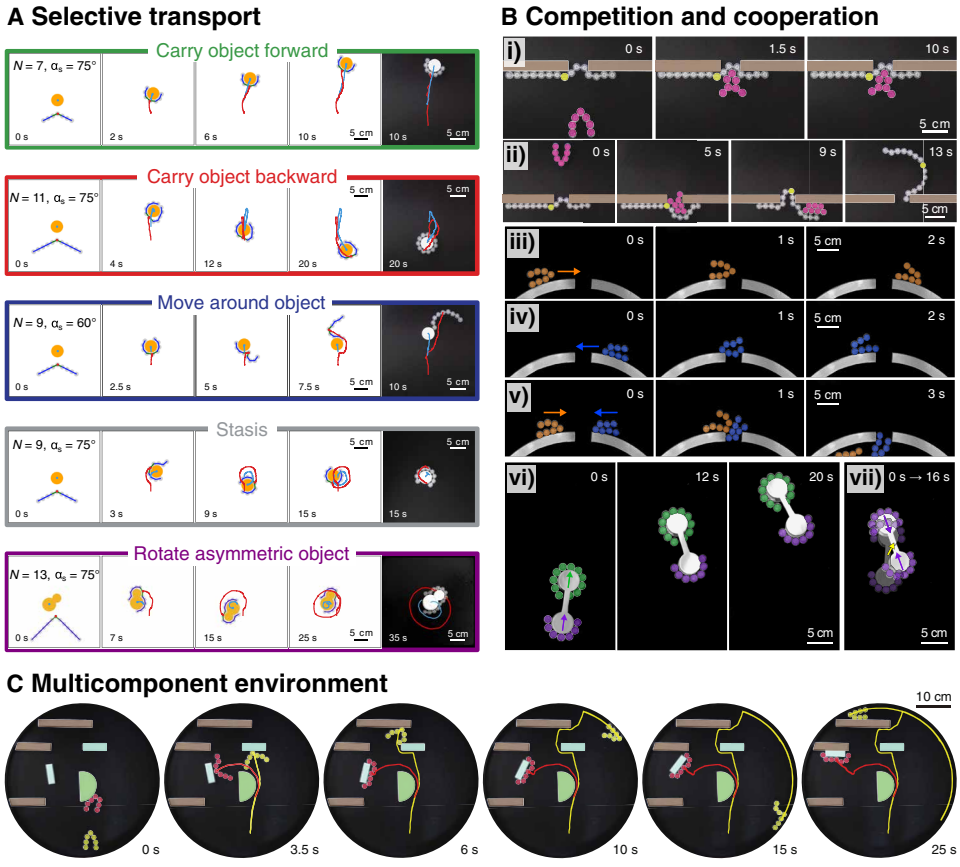

Fig. 4. Link-bots perform selective transportation and dynamic social interactions. (**A**) A link-bot can push, pull, bypass, wrap, and rotate a passive object ($d_{obj} = 2.67d$). The link-bot trajectory is shown in red, and the object trajectory is shown in blue. The last snapshot in each panel shows the analogous experiment. (**B**) Two link-bots (gray: $N = 15$, $\theta_c = 90°$, $\alpha_s = 75°$; pink: $N = 7$, $\theta_c = 20°$, $\alpha_s = 15°$) interact at a gap in a wall either competitively so that both link-bots are stuck (i) or cooperatively so that both pass through the gap (ii). Individual link-bots ($\theta_c = 20°$, $\alpha_s = 15°$) moving in the translation gait (iii and iv) cross over the gap in a wall. When moving simultaneously (v), these link-bots cooperate to pass through the gap together. (vi) A dumbbell-shaped object is carried by the cooperation of one link-bot pushing (purple; arrow shows direction of link-bot propulsion) and another pulling (green). The link-bots have the same link angles ($\theta_c = 90°$, $\alpha_s = 75°$) but are made up of a different number of bots. (vii) Overlapped images of a dumbbell-shaped object interacting with identical link-bots whose 4competing pushing forces cause the object to stay nearly stationary. (**C**) Two link-bots (yellow: $\theta_c = 30°$, $\alpha_s = 30°$; red: $\theta_c = 60°$, $\alpha_s = 40°$) show different functions in an environment containing curved walls, straight walls, and moveable objects.

remains wrapped around the object in a state of stasis, with no substantial translational movement. When the object has a pronounced asymmetry, the link-bot is able to rotate it. These trends are similar across angular constraints, with carrying behaviors enhanced by high side-chain flexibility at high α_s values and object avoidance behaviors promoted by rigid side chains at low α_s values (phase diagrams and momentum analysis shown in fig. S17). These selective transportation behaviors predicted by the simulated link-bot are observed in experimental studies, shown as complementary final time point snapshots in Fig. 4A and in more detail in fig. S16 and movie S4. The link-bot is not limited to interactions with a circular object. With sufficiently large N, θ_c, and α_s, a link-bot can enclose objects of diverse shapes, including ellipses, squares, triangles, L-shapes, and cross shapes (fig. S18 and movie S4).

To explore competitive and cooperative behaviors experimentally, we consider how two link-bots hinder or promote movement in two different environments: through a gap in a wall or transporting an object. In one scenario at a wall, a long link-bot, colored gray in Fig. 4B, is engaged in an exploitative stationary gait at the gap, and the direction of an approaching link-bot, colored pink, determines the nature of their interaction. In the competitive case (i), both link-bots push into the wall together and both become jammed at the gap. In the cooperative case (ii), the pink link-bot is able to overcome the self-propulsion forces of the gray one and helps both pass through by realigning the gray link-bot with the gap. More details are shown in fig. S10. In another scenario, when a single link-bot in the translation gait moves along a wall, it crosses over the gap regardless of whether it is traveling left to right (iii) or right to left (iv). However, when these link-bots translate simultaneously such that they meet at the gap coming from opposite directions, they cooperatively reorientate toward the wall and both pass through the gap. This highlights that cooperation or competition is not merely dependent on whether the two link-bots are initialized on the same or opposite sides of the wall. The collective movement of a dumbbell-shaped object by two link-bots takes advantage of the fact that link-bots are able to pull or push an object. When a link-bot that pushes is paired and aligned with a link-bot that pulls, they will cooperatively move an object (vi), while two link-bots that push will provide

Downloaded from https://www.science.org at Seoul National University Library on May 11, 2025

competing forces to cancel out transporting behavior and keep the object stationary (vii).

DISCUSSION

Link-bots provide a simple modular approach to investigate an analog of an active polymer chain, made of bots, that can locomote, navigate, transport, and interact in a variety of environments. By manipulating a few internal geometric constraints, these link-bots show functionality and versatility that have been a challenge to achieve in traditional robotic swarms without sophisticated control. This is explained by the ways the deformable, active structure of the link-bot allows for breathing and flapping movement modes, which produce three gaits at a boundary. Advanced behavior does not require increased complexity at the link-bot level but comes from complexity in the environment. We emphasize that the link-bot is able to perform a wide variety of functions with minimal control, with even more behaviors to be explored. This is shown through a range of contrasting tasks including navigating through or circumventing obstacles, adhering to or detaching from objects, transporting objects in forward or backward directions, traversing or blocking small gaps, allowing or obstructing the passage of objects through gaps, and self-sorting on a curved surface. Figure 4C shows an example where these behaviors are exhibited in a multicomponent environment (see also fig. S19 and movie S5).

The experimental system in this work is limited by its dependence on a vibrating surface as an external global stimulus for bot activity, which affects all bots uniformly. Although the computational model addresses this by allowing individual control of self-propulsion and noise, it simplifies interactions by excluding explicit friction forces that affect the quantitative details of link-bot dynamics when investigating beyond their gait types. Additional further work could extend the capabilities of the link-bot by making the links and crests dynamically adjustable. The ability to modify link and crest shapes and material properties, using environmental conditions for example, would allow for a broader range of movements and remotely controlled on-the-fly transformations. Leveraging its potential for extensibility, the link-bot principle of using geometric constraints between active bots can serve as a starting point for developing versatile and minimalistic robot collectives across various scales. These principles could also be applied to develop robust and cost-effective robots for tasks such as transporting goods over challenging terrain, conducting environmental surveillance, or controlling traffic flow. Our findings provide valuable insight into the development of multifunctional robotic systems that are both resource-efficient and scalable, with the potential to impact a wide range of industries and activities.

METHODS

Experiments

Link-bot fabrication

As shown in Fig. 1A, each bot comprises two cylinders, the cap (diameter, 15 mm; height, 6.5 mm) and the body (diameter, 8 mm; height, 6.5 mm), and a cuboid top (width, 1.5 mm; length, 5 mm; height, 8 mm) on the cap, all three of which are connected on the same axis. The cap is equipped with seven legs (length, 8 mm; diameter, 1 mm) that are tilted at an angle of 10° from the vertical direction. The connecting link (thickness, 1.5 mm) consists of two disks (diameter, 8.5 mm) joined by a bar (length, 16 mm; width, 2.5 mm). The length L slightly exceeds d, allowing the creation of a chain without direct contacts between adjacent bots. Each disk features a ribbon-shaped notch that allows the cuboid crest of the bot to rotate freely within a prescribed angle, and the two notches in the link have the same orientation. To fabricate all bots and links, a transparent photopolymer with an acrylate base is used, using stereolithography three-dimensional printing that has an accuracy of approximately ±0.1 mm (Formlabs Form 3). For the analysis of the link-bot's travel distance, velocity, and trajectory, we trace and examine the position of the center bot using the TrackMate plug-in for ImageJ (*37*).

Vibrating table

The bots are subjected to excitation through the vertical vibration of a circular acrylic base plate (diameter, 480 mm; height, 30 mm), firmly mounted on an electromagnetic shaker (Tira TV 5220). The plate is maintained in a horizontal position with a precision of 0.1°. The motion of the bots is confined within a circular boundary (diameter, 450 mm). To mitigate resonance effects, the shaker is attached to massive concrete blocks. Experiments are carried out with vibrations at a frequency of 80 Hz and an amplitude of 70 μm, ensuring a consistent and steady excitation of the bots.

Computational model

Bot activity

A model was created using Python to simulate link-bot behavior to investigate detailed properties and extend the parameter scope. The link-bot is modeled as a collective of N active Brownian particles interacting through constraints imposed by the connecting links and the surrounding environment. Each circular bot i has position $\mathbf{r}_i$ and orientation ϕ_i at time t, shown in Fig. 5A, which are updated according to the following dynamical update rule

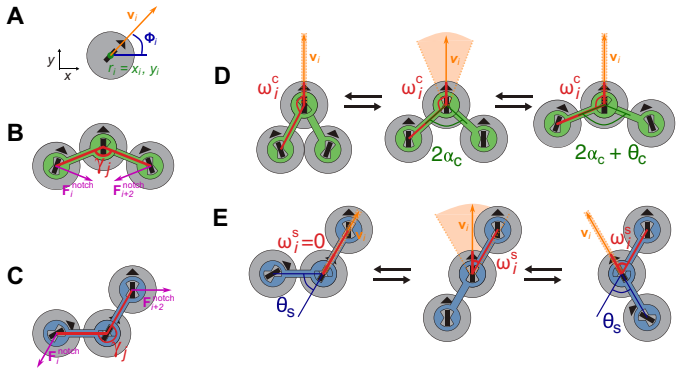

Fig. 5. Schematic representation of the angles and vectors in the link-bot model. (**A**) Position and velocity vector of a single bot. Schematics of a partial link-bot showing the translational forces, $\mathbf{F}^{notch}$, due to the link notch angle for (**B**) bots connected by center links and (**C**) bots connected by side links in the case where $j = i + 1$. Pictured here is a side chain to the left of the center bot, which is flapping outward. For the case where the side chain flaps inward, the results are mirrored. For both the center and side links, $\mathbf{F}^{notch} > 0$ only when $\gamma_j > \gamma_{max}$. The notches constrain bot rotation for (**D**) the center bot and (**E**) the side bots. In the neutral configuration (shown in the middle), the bots have maximum rotational freedom, shown by a shaded orange region. When the bots are in their fully extended breathing and flapping modes (shown for both directions on either side), the bots have no rotational freedom.

Downloaded from https://www.science.org at Seoul National University Library on May 11, 2025

$$\mathbf{v}_i^t = \mathbf{v}_i^{t-1} + \Bigg[\underbrace{\sum_{j=1}^{N} \mathbf{F}_{i,j}^{\text{overlap}}}_{\text{forces due to bot–bot interactions}} + \underbrace{\mathbf{F}_{i,j=i-1}^{\text{link}} + \mathbf{F}_{i,j=i+1}^{\text{link}}}_{\text{forces due to rigid link length}} + \underbrace{\mathbf{F}_{i,j=i-1}^{\text{notch}} + \mathbf{F}_{i,j=i+1}^{\text{notch}}}_{\text{forces due to link notch constraints}} \Bigg] \mathrm{d}t \quad (1)$$

where the velocity of the bot at time $(t-1)$ is given by

$$\mathbf{v}_i^{t-1} = v_0 \begin{bmatrix} \cos\phi_i \\ \sin\phi_i \end{bmatrix} + \sqrt{2D}\eta_i \quad (2)$$

Here, bot activity is given by a constant self-propulsion speed v_0, the diffusion coefficient D, and a noise array randomly sampled from standard normal distribution η_i (Eq. 2). More information about how D is calibrated from experiments is given in fig. S1. We observe experimentally that the bots move primarily along via translation and do not rotate without translation, i.e., they are subject to a nonholonomic constraint (*38*). This coupling of the orientational movement to translation is likely due to the fact that the bot motion is generated tangential to the leg tilt direction on the vibrating surface. Therefore, the noise in the model is applied to translation of the bot rather than rotation, which is seen to provide appropriate dynamics. Some quantitative differences can be observed in freely moving link-bots if noise is applied to both rotation and translation (for example, in the relaxation to the V-shaped neutral configuration), but no substantial differences were seen in the gaits and dynamics reported in this work.

Link constraints

The forces acting on each bot due to its connecting link(s) and any external constraints are implemented using the geometry of the link-bot with respect to the position of the bots. The rigidity of each bot and the connecting links are maintained through linear spring constraints

$$\mathbf{F}_{i,j}^{(\cdot)} = -k\left(r_{i,j} - r_0\right)\hat{r}_{i,j} \quad (3)$$

where $r_{i,j}$ is the distance between bot i and bot j, $\mathbf{F}_{i,j}^{\text{overlap}}$ uses $r_0 = d$, and $\mathbf{F}_{i,j}^{\text{link}}$ uses $r_0 = L$.

All spring constants are set to a sufficiently high value, $k = 2 \times 10^5$ N/m. Wall and object boundary constraints are implemented as perfectly elastic collisions.

The link notches are a key feature of the link-bot, providing a hard boundary that affects both bot translation and rotation. These constraints cause each bot's movement to be coupled with the relative positions of its neighboring bots. This is enhanced by the fact that all bots, except for the side bots at the end of the chains, are controlled by two overlapping links. This feature contributes to the emergent complex behaviors of the link-bot.

The translational constraints imposed on each bot i by the link notches are implemented as an exponential spring, which is dependent on the angles of the links between bots $i \pm 1$ and $i \pm 2$. Figure 5 (B and C) provides schematics of these angles and forces for sample partial link-bots

$$\mathbf{F}_{i,j=i-1}^{\text{notch}} = -k\exp\left(\gamma_{j=i-1} - \gamma_{\max}\right) H\left(\gamma_{j=i-1} - \gamma_{\max}\right)\hat{r}_{j=i-1,i-2} \quad (4)$$

$$\mathbf{F}_{i,j=1+1}^{\text{notch}} = -k\exp\left(\gamma_{j=i+1} - \gamma_{\max}\right) H\left(\gamma_{j=i+1} - \gamma_{\max}\right)\hat{r}_{j=i+1,i+2} \quad (5)$$

Table 1. Parameters used in link-bot model with typical values.

Parameter	Description	Typical value(s)	Unit
d	Bot diameter	1.5	cm
v_0	Bot self-propulsion speed	8	cm/s
D	Bot diffusion coefficient	10	cm^2/s
L	Link length	1.6	cm
θ_c	Center link notch angle*	10–180	degrees
α_c	Center link spread angle	10–90	degrees
θ_s	Side-link notch angle	60	degrees
α_s	Side-link spread angle*	10–90	degrees
k	Spring constant	2×10^5	N/m
N	Number of bots in a link-bot	3–33	–
$\mathrm{d}t$	Time step	1×10^{-3}	s
b	Gap in wall spacing	3–6	cm
x	Channel spacing	3	cm
z	Broken wall spacing	3–7.5	cm
r	Radius of curved wall	3–15	cm
d_{obj}	Object diameter	1.5–15	cm

*Parameter that strongly controls gait.

Downloaded from https://www.science.org at Seoul National University Library on May 11, 2025

where γ_j is the angle made by the two links connected to bot j (which is offset by ±1 from bot i) and γ_{max} is a maximum angle constraint set by the notches. For the center bot, $\gamma_{max} = 2\alpha_c + \theta_c$, and for the side bots, $\gamma_{max} = 180° + \theta_s$. The Heaviside step function $H\left(\gamma_j - \gamma_{max}\right)$ ensures that the bots move freely except when the limits of the notch are reached. Figure 5 (B and C) provide schematics of these angles and forces for sample partial link-bots.

The rotational boundaries felt by each bot due to its one or two overlapping link notches are implemented as hard angle constraints on the bot velocity vector. Equations 6 and 7 show these clamped angle limits for center and side bots when situated in a neutral configuration with their neighbors (i.e., all crests are aligned), as shown in the middle schematic of Fig. 5 (D and E)

$$\omega_i^c = \max\left\{180° - \alpha_c - \theta_c/2, \min\left(\omega_i^c, 180° - \alpha_c + \theta_c/2\right)\right\} \quad (6)$$

$$\omega_i^s = \max\left\{\alpha_s - \theta_s/2, \min\left(\omega_i^s, \alpha_s + \theta_s/2\right)\right\} \quad (7)$$

where ω_i^c is the angle between the center bot crest and its neighboring link to the left and ω_i^s is the angle between the side bot crest and its neighboring link above (closer to the center bot). When the link-bot engages in breathing or flapping movements, the notches on the bots move in opposite directions and lead to increased constraint of the bot rotation. This is shown in Fig. 5 (D and E) in the minimally and maximally extended cases in which the bot has no rotational freedom. For example, when the link-bot center V-angle is at its maximum value of $2\alpha_c + \theta_c$, the center bot's orientation is completely constrained since the two notches surrounding its crest are fully rotated in opposite directions. In this situation, the center bot cannot rotate and points straight forward relative to the link-bot V-shape ($\omega^c = 180° - \alpha_c - \theta_c/2$). The main parameters of the model and their typical values are provided in Table 1.

Supplementary Materials

The PDF file includes:
Supplementary Text
Figs. S1 to S19
Legends for movies S1 to S5

Other Supplementary Material for this manuscript includes the following:
Movies S1 to S5

REFERENCES AND NOTES

1. M. Rubenstein, A. Cornejo, R. Nagpal, Programmable self-assembly in a thousand-robot swarm. *Science* **345**, 795–799 (2014).
2. I. Slavkov, D. Carrillo-Zapata, N. Carranza, X. Diego, F. Jansson, J. Kaandorp, S. Hauert, J. Sharpe, Morphogenesis in robot swarms. *Sci. Robot.* **3**, eaau9178 (2018).
3. L. Giomi, N. Hawley-Weld, L. Mahadevan, Swarming, swirling and stasis in sequestered bristle-bots. *Proc. R. Soc. A Math. Phys. Eng. Sci.* **469**, 20120637 (2013).
4. A. E. Turgut, H. Çelikkanat, F. Gökçe, E. Şahin, Self-organized flocking in mobile robot swarms. *Swarm Intell.* **2**, 97–120 (2008).
5. F. A. Lavergne, H. Wendehenne, T. Bäuerle, C. Bechinger, Group formation and cohesion of active particles with visual perception–dependent motility. *Science* **364**, 70–74 (2019).
6. H. R. Vutukuri, M. Lisicki, E. Lauga, J. Vermant, Light-switchable propulsion of active particles with reversible interactions. *Nat. Commun.* **11**, 2628 (2020).
7. J. Zhang, F. Mou, Z. Wu, J. Song, J. E. Kauffman, A. Sen, J. Guan, Cooperative transport by flocking phototactic micromotors. *Nanoscale Adv.* **3**, 6157–6163 (2021).
8. A. Aghakhani, O. Yasa, P. Wrede, M. Sitti, Acoustically powered surface-slipping mobile microrobots. *Proc. Natl. Acad. Sci. U.S.A.* **117**, 3469–3477 (2020).
9. J. Yu, B. Wang, X. Du, Q. Wang, L. Zhang, Ultra-extensible ribbon-like magnetic microswarm. *Nat. Commun.* **9**, 3260 (2018).
10. W. Wang, G. Gardi, P. Malgaretti, V. Kishore, L. Koens, D. Son, H. Gilbert, Z. Wu, P. Harwani, E. Lauga, C. Holm, M. Sitti, Order and information in the patterns of spinning magnetic micro-disks at the air-water interface. *Sci. Adv.* **8**, eabk0685 (2022).
11. S. Ceron, G. Gardi, K. Petersen, M. Sitti, Programmable self-organization of heterogeneous microrobot collectives. *Proc. Natl. Acad. Sci. U.S.A.* **120**, e2221913120 (2023).
12. H. Xie, M. Sun, X. Fan, Z. Lin, W. Chen, L. Wang, L. Dong, Q. He, Reconfigurable magnetic microrobot swarm: Multimode transformation, locomotion, manipulation. *Sci. Robot.* **4**, eaav8006 (2019).
13. G. Gardi, S. Ceron, W. Wang, K. Petersen, M. Sitti, Microrobot collectives with reconfigurable morphologies, behaviors, functions. *Nat. Commun.* **13**, 2239 (2022).
14. V. Narayan, S. Ramaswamy, N. Menon, Long-lived giant number fluctuations in a swarming granular nematic. *Science* **317**, 105–108 (2007).
15. A. Deblais, T. Barois, T. Guerin, P.-H. Delville, R. Vaudaine, J. S. Lintuvuori, J.-F. Boudet, J.-C. Baret, H. Kellay, Boundaries control collective dynamics of inertial self-propelled robots. *Phys. Rev. Lett.* **120**, 188002 (2018).
16. J.-F. Boudet, J. Lintuvuori, C. Lacouture, T. Barois, A. Deblais, K. Xie, S. Cassagnere, B. Tregon, D. B. Brückner, J.-C. Baret, H. Kellay, From collections of independent, mindless robots to flexible, mobile, directional superstructures. *Sci. Robot.* **6**, eabd0272 (2021).
17. W. Savoie, T. A. Berrueta, Z. Jackson, A. Pervan, R. Warkentin, S. Li, T. D. Murphey, K. Wiesenfeld, D. I. Goldman, A robot made of robots: Emergent transport and control of a smarticle ensemble. *Sci. Robot.* **4**, eaax4316 (2019).
18. S. Li, R. Batra, D. Brown, H.-D. Chang, N. Ranganathan, C. Hoberman, D. Rus, H. Lipson, Particle robotics based on statistical mechanics of loosely coupled components. *Nature* **567**, 361–365 (2019).
19. S. Li, B. Dutta, S. Cannon, J. J. Daymude, R. Avinery, E. Aydin, A. W. Richa, D. I. Goldman, D. Randall, Programming active cohesive granular matter with mechanically induced phase changes. *Sci. Adv.* **7**, eabe8494 (2021).
20. Y. Xi, T. J. Jones, R. Huang, T. Marzin, P.-T. Brun, Emergent intelligence of buckling-driven elasto-active structures. arXiv:2404.10614 [cond-mat.soft] (2024).
21. M. Spellings, M. Engel, D. Klotsa, S. Sabrina, A. M. Drews, N. H. Nguyen, K. J. Bishop, S. C. Glotzer, Shape control and compartmentalization in active colloidal cells. *Proc. Natl. Acad. Sci. U.S.A.* **112**, E4642–E4650 (2015).
22. C. Scholz, A. Ldov, T. Pöschel, M. Engel, H. Löwen, Surfactants and rotelles in active chiral fluids. *Sci. Adv.* **7**, eabf8998 (2021).
23. M. Agrawal, S. C. Glotzer, Scale-free, programmable design of morphable chain loops of kilobots and colloidal motors. *Proc. Natl. Acad. Sci. U.S.A.* **117**, 8700–8710 (2020).
24. L. Caprini, I. Abdoli, U. M. B. Marconi, H. Löwen, Spontaneous self-wrapping in chiral active polymers. arXiv:2410.02567 [cond-mat.soft] (2024).
25. Y. Ozkan-Aydin, D. I. Goldman, Self-reconfigurable multilegged robot swarms collectively accomplish challenging terradynamic tasks. *Sci. Robot.* **6**, eabf1628 (2021).
26. M. Kulkarni, H. Nguyen, K. Alexis, The reconfigurable aerial robotic chain: Shape and motion planning. *IFAC Pap. OnLine* **53**, 9295–9302 (2020).
27. P. Friedl, D. Gilmour, Collective cell migration in morphogenesis, regeneration and cancer. *Nat. Rev. Mol. Cell Biol.* **10**, 445–457 (2009).
28. T. Vicsek, A. Zafeiris, Collective motion. *Phys. Rep.* **517**, 71–140 (2012).
29. J. W. Boley, W. M. Van Rees, C. Lissandrello, M. N. Horenstein, R. L. Truby, A. Kotikian, J. A. Lewis, L. Mahadevan, Shape-shifting structured lattices via multimaterial 4D printing. *Proc. Natl. Acad. Sci. U.S.A.* **116**, 20856–20862 (2019).
30. Z. Hao, S. Mayya, G. Notomista, S. Hutchinson, M. Egerstedt, A. Ansari, Controlling collision-induced aggregations in a swarm of micro bristle robots. *IEEE Trans. Robot.* **39**, 590–604 (2023).
31. T. Xu, C. Qin, B. Tang, J. Gao, J. Zhou, K. Chen, T. H. Zhang, W. Tian, Constrained motion of self-propelling eccentric disks linked by a spring. *J. Chem. Phys.* **161**, 064905 (2024).
32. E. Zheng, M. Brandenbourger, L. Robinet, P. Schall, E. Lerner, C. Coulais, Self-oscillation and synchronization transitions in elastoactive structures. *Phys. Rev. Lett.* **130**, 178202 (2023).
33. Y. Xia, Z. Hu, D. Wei, K. Chen, Y. Peng, M. Yang, Biomimetic synchronization in biciliated robots. *Phys. Rev. Lett.* **133**, 048302 (2024).
34. I. L. Bajec, F. H. Heppner, Organized flight in birds. *Anim. Behav.* **78**, 777–789 (2009).
35. R. G. Winkler, J. Elgeti, G. Gompper, Active polymers–emergent conformational and dynamical properties: A brief review. *J. Physical Soc. Japan* **86**, 101014 (2017).
36. R. Chelakkot, A. Gopinath, L. Mahadevan, M. F. Hagan, Flagellar dynamics of a connected chain of active, polar, Brownian particles. *J. R. Soc. Interface* **11**, 20130884 (2014).
37. J.-Y. Tinevez, N. Perry, J. Schindelin, G. M. Hoopes, G. D. Reynolds, E. Laplantine, S. Y. Bednarek, S. L. Shorte, K. W. Eliceiri, Trackmate: An open and extensible platform for single-particle tracking. *Methods* **115**, 80–90 (2017).
38. A. M. Bloch, *Nonholonomic Mechanics* (Springer, 2015).

Acknowledgments

Funding: This work was supported by the National Research Foundation of Korea (grant nos. 2018-052541 and 2021-017476) via the SNU SOFT Foundry Institute. H.-Y.K. acknowledges

Downloaded from https://www.science.org at Seoul National University Library on May 11, 2025

administrative support from SNU Institute of Engineering Research. K.B. acknowledges support from the Human Frontier Science Program grant LT000444/2021-C. **Author contributions:** Conceptualization: K.S., K.B., H.-Y.K., and L.M. Experiments: K.S. and K.K. Computations: K.B. Analysis and interpretation: K.B., L.M., K.S., and H.-Y.K. Visualization: K.B. and K.S. Supervision: H.-Y.K. and L.M. Writing—original draft: K.S. and K.B. Writing—review and editing: K.B., H.-Y.K, and L.M. **Competing interests:** H.-Y.K. and K.S. are inventors on the patent application (#10-2023-0186386, Republic of Korea) submitted by SNU R&DB Foundation that covers the design of self-propelled particles and links, as well as the method for configuring a multifunctional particle chain system using them. The authors declare that they have no other competing interests. **Data and materials availability:** All data needed to evaluate the conclusions in the paper are present in the paper and/or the Supplementary Materials.

Submitted 22 November 2024
Accepted 4 April 2025
Published 9 May 2025
10.1126/sciadv.adu8326

Downloaded from https://www.science.org at Seoul National University Library on May 11, 2025

Science Advances
AAAS

Supplementary Materials for

Emergent functional dynamics of link-bots

Kyungmin Son *et al.*

Corresponding author: L. Mahadevan, lmahadev@g.harvard.edu; Ho-Young Kim, hyk@snu.ac.kr

Sci. Adv. **11**, eadu8326 (2025)
DOI: 10.1126/sciadv.adu8326

The PDF file includes:

Other Supplementary Material for this manuscript includes the following:

1. Single bot

Individual bots in this work are like the bristle-bots investigated in previous studies [3], with the distinction that the mechanical energy source comes from the vibration of the arena surface rather than the bot vibrating internally. This means that variability in activity is not prescribed at the individual bot level, although it is observed here.

The noisy movement of a bot in this experimental system is inherent, due to slight environmental variations (such as humidity) and imperfections in the bot and surface features at a small scale. To incorporate this noise within the computational model, the diffusion coefficients of a single bot are calculated from 11 experimental runs in which the bot moves freely on a vibrating surface, without interactions from other bots or walls, and the resulting average value of 10 cm^2/s is used as the noise term D within the model, as shown in Equation 2. To validate this parameter, translational diffusion coefficients were calculated from another experiment and a simulation using $D = 10\ \mathrm{cm}^2/\mathrm{s}$, each 20 seconds long. The observed experimental translational diffusion coefficient, $D_{\mathrm{obs}}^{\mathrm{exp}} = 12.24\ \mathrm{cm}^2/\mathrm{s}$ (Fig. S1(a)) and observed simulated translational diffusion coefficient of $D_{\mathrm{obs}}^{\mathrm{sim}} = 12.22\ \mathrm{cm}^2/\mathrm{s}$ (Fig. S1(b)) are in good agreement .

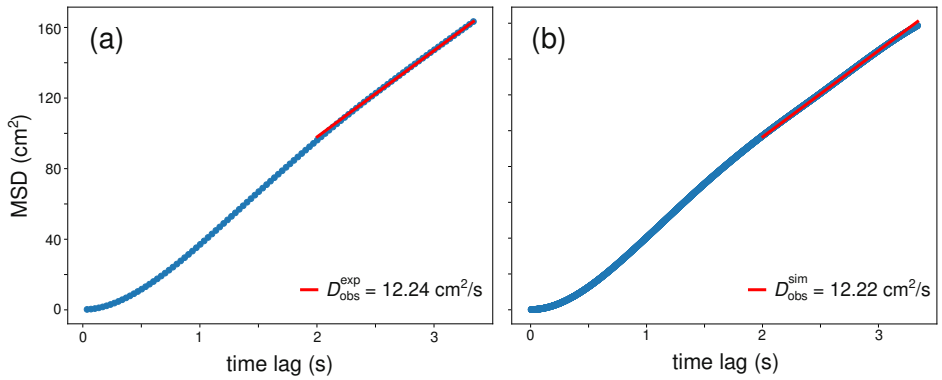

Fig. S1. **Observed diffusion coefficients in experiment and simulation.** The observed translational diffusion coefficients, D_{obs}, determined from 20 second trajectories of a single bot obtained from (**a**) experiment and (**b**) simulation show good agreement when the model noise parameter is set to $D = 10\ \mathrm{cm}^2/\mathrm{s}$.

2. Link angles

The link angles α and θ are essential parameters that determine the gaits and subsequent behaviors of link-bots. Fig. S2 summarizes the role of each of the critical link angles on the resulting whole link-bot neutral configuration and dynamic flexibility.

α values indicate the link spread angles. They determine the geometric flexibility of the link-bot by defining the neutral positions of the links in relation to bot orientation. Low α values create a compact neutral configuration where the links are closely aligned with the direction of the bot orientation, while high α values lead to a link-bot neutral configuration that is spread out.

α_c controls the neutral alignment of the center links. Since there are only two center links in all the link-bots studied in this work, this value is fixed by the bot parameters d, L, and θ_c.

α_s controls the neutral configuration of the side chains and therefore sets the extent to which they are spread out at an angle with the forward direction or compact in line with the forward direction.

θ values represent the angles of link notches. They determine the dynamic flexibility of the link-bot, allowing for significant bot movement and rotation with high θ values or minimal movement and rotation with low θ values.

θ_c controls the central angle of the link-bot and therefore this angle directly sets the breathing angle range.

θ_s sets the side link notch angles and therefore controls the rigidity of the side chains.

Both α_s and θ_s influence the flexibility of the side chains and they show similar effects on link-bot behaviors (see Section S 6 for more details). Therefore, in most cases it is sufficient to control only one of these parameters. α_c is not set as a separate parameter, but θ_c is a critical value to control the dynamics around the central bot. In this work, α_s and θ_c are the essential parameters used to control the link-bot gait and its corresponding behavior in complex environments.

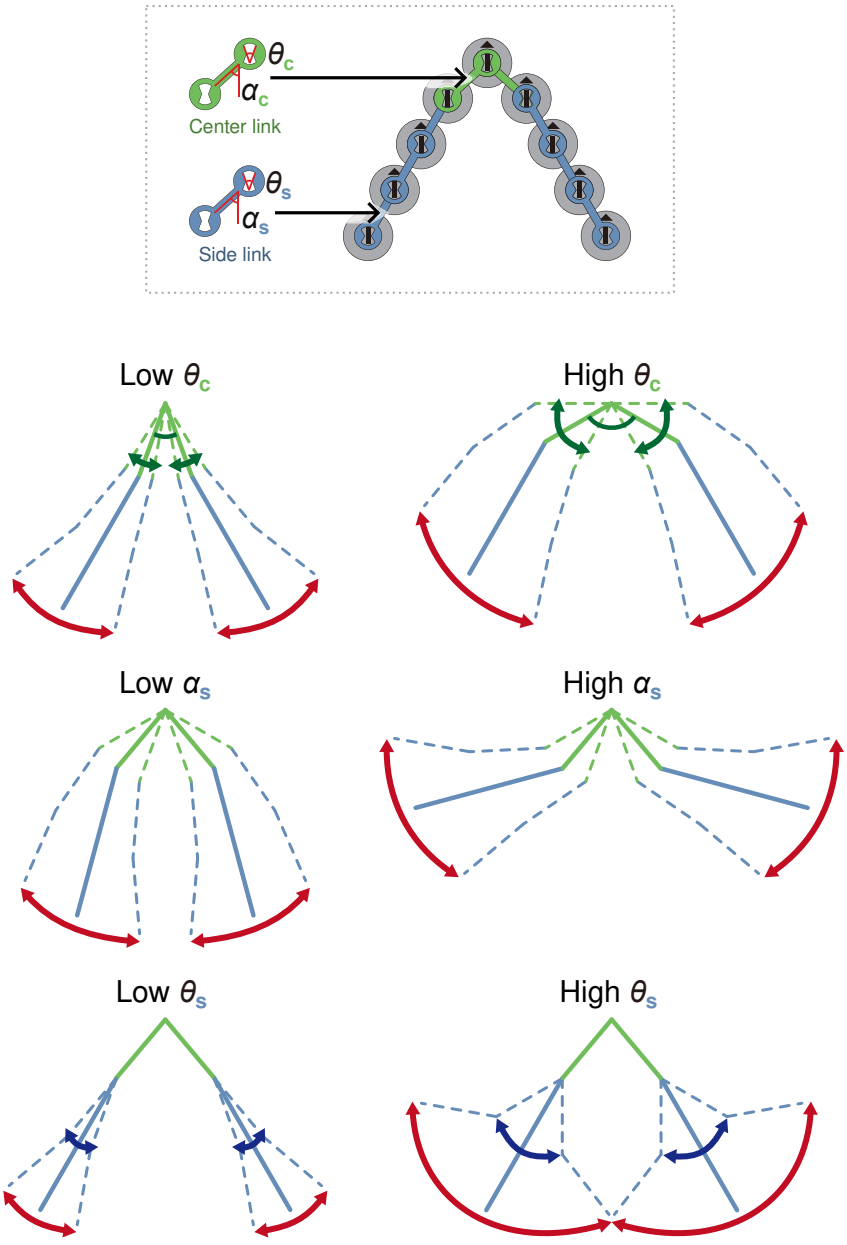

Fig. S2. **Schematic of link-bot configuration and dynamics with respect to link angles.** The link angles θ_c, α_s, and θ_s are vital parameters in controlling the link-bot geometry and dynamics. This schematic shows representative neutral configurations and dynamic modes caused by high or low values of the link notch and spread angles. Center links are represented as green lines, with the corresponding breathing movement mode indicated with green arrows. The side links are represented as blue lines and the flapping movement mode is shown using blue arrows.

3. Link-bot with no angular constraints

Figure S3 shows the experimental behavior of a link-bot consisting of $N = 7$ bots connected by links with $\theta_c = \theta_s = 180°$, allowing free rotation of each bot and link. In this case, we initially orient the bots in one direction so that the link-bot travels to the boundary of a diameter arena $\geq 20d$. Upon reaching the boundary, the link-bot randomly deforms and repeatedly detaches and reattaches to the wall. In this case, one or both ends of the link-bot must be pinned or clamped in order to observe directed or periodic motion, such as in [31]. This is in contrast to the cases investigated more thoroughly in this work, where the bots possess some angular constraints due to the link angles (for example, with link parameters of $\theta_c = 40°$, $\theta_s = 60°$, $\alpha_s = 30°$). In these cases, the link angle constraints promote orientational alignment of the bots which, along with the symmetrical structure of the link-bot, allow it to maintain its movement along a boundary.

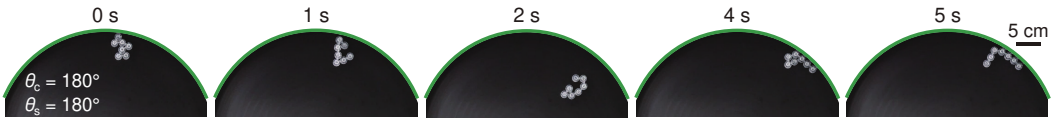

Fig. S3. **Rotationally free link-bot at wall** A link-bot that is connected with links possessing no angular constraints on the self-propelled bots shows no directed or consistent movement, even at a wall.

4. Mechanics of link-bot gaits

Due to the symmetric V-shaped configuration of the link-bot, the orientation and motion of its center bot indicates the movement of the link-bot as a whole. However, it is worth emphasizing that the central bot has no enhanced features or control compared to the side bots, and its behavior is strongly coupled to the positions and motion of the side bots through the constraining links. Understanding the mechanics of the gaits thus requires consideration of how the side bots influence behavior of the center bot. A key feature distinguishing the gaits is the relative movement of the two link-bot side chains relative to the center bot, and in particular the torque felt by the center bot from the forces applied by the active side chains. In all gaits, the center bot and at least one side chain are in continuous contact with the boundary wall.

a. Translation gait

In the translation gait, both side chains remain close together as the link-bot moves. This means that the forces exerted by the side bots on the center bot through the links are largely translational, with no large torques applied, and therefore no orientational changes occur. This gait thus dominates when θ_c is small ($\theta_c < 30°$), since this constraint directly limits the maximum allowable breathing angle and causes the center links to remain folded in an acute angle.

b. Oscillation gait

The oscillation gait is a rich emergent behavior of the loosely constrained active bots. When the side chains can move apart significantly and/or are highly flexible (causing high breathing and flapping movements, respectively), the side bots can exert a high torque on the center bot. This torque causes the rotation of the center bot and the subsequent flipping of the link-bot characteristic of the oscillation gait. This relative movement of the side chain is modulated by the link angles: an intermediate θ_c value ($30° < \theta_c < 50°$) causes a large breathing angle and α_s values above a threshold ($\alpha_s > 10°$) increase side chain flexibility. One contributing factor to the link-bot dynamics and the high torque around the center bot is the fact that when the two bots on either side of the center bot are maximally flexed, the

link notches are rotated such that the center bot has no independent freedom of rotation. In this case, any orientational change that the center bot undergoes will directly affect the positions of its neighboring linked bots. This occurs when any three linked bots are minimally or maximally flexed (as shown for bots connected by center links and side links in Fig. 5D and E, respectively), although the effects are most noticeable with the center bot since it has the strongest effect on the link-bot orientation.

The cyclic reorientation process involves the following steps: (1) the movement of bots not interacting with the boundary opens the center of the link-bot to its maximum angle θ_{M}, (2) the torque generated by this sustained movement induces rotation of the center bot, and (3) the remaining bots then move away from the boundary, causing the link-bot to reverse its direction. This is illustrated in Fig. S4. Starting from panel 1, the link-bot is initially moving to the right with one side chain (indicated in yellow) in contact with the boundary wall. Bots interacting with the boundary are subjected to greater friction and normal forces than distant ones, enhanced by the notch angular constraints which often keep them pointing towards the wall. After some time, the bots distant from the boundary (colored blue) catch up with the yellow ones , and the center of the link-bot spreads to its maximum angle of θ_{M}, seen in Fig. S4A panel 2. The blue bots stop the center bot (colored red) and all bots cause it to rotate, as the yellow and blue bots move to detach from and attach to the boundary, respectively (panel 4). The link-bot has now reversed its translational direction from traveling right to traveling to the left (panels 5-8). We note that this reorientation starts when the center bot is stopped by the side chain further from the wall, which is only possible when the maximum spread angle of the center link is greater than the right angle, $\theta_{\mathrm{M}} > 90°$, or when the further side chain can move in front of the center bot. Therefore, by adjusting the link parameter α_{c} so that θ_{M} crosses 90°, we can produce a significant change in the link-bot's interactions with a wall, from the translation to the oscillation gait. This reorientation is not observed at low θ_{c} values due to the small torque acting on the center bot when the central angle spreads only narrowly.

c. Stationary gait

If the side chains are able to move significantly far apart such that they can independently interact with the boundary, then the torques they generate will balance in opposite

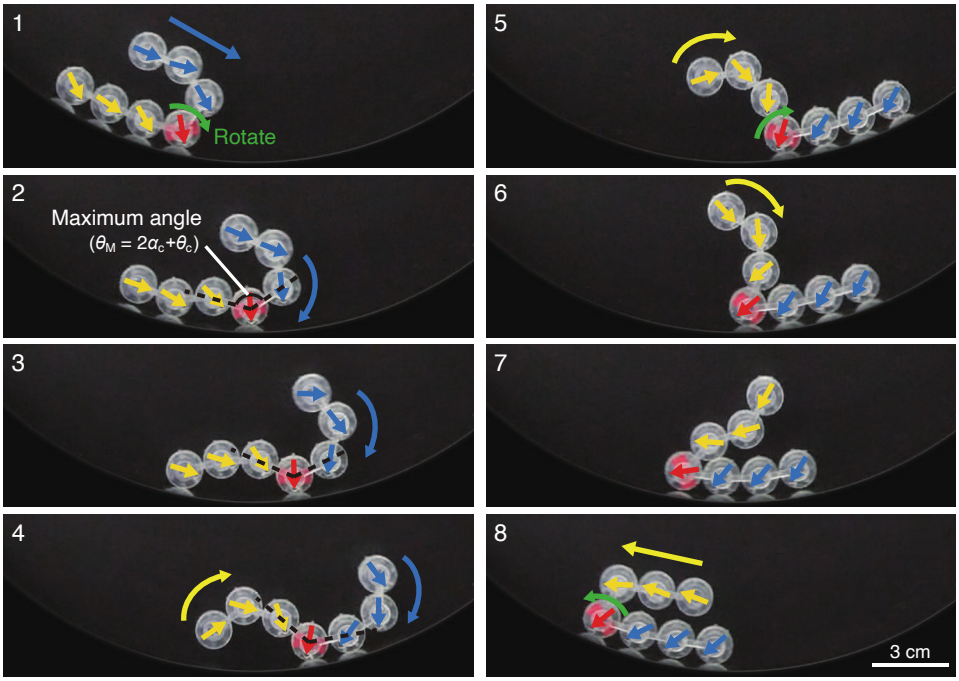

Fig. S4. **The mechanism of directional change at a wall.** The directional change process of a link-bot with $\theta_c = 40°$, $\theta_s = 60°$, $\alpha_s = 30°$. The relatively high translation of the bots on the side chain that is further from the wall (shown in blue for the initial panels) increases the angle between the two center links, causing the side chain to rotate and reverse the center bot's translation direction. The orientation of each bot is indicated by the marked arrows.

directions and the link-bot will remain immobile at the wall, entering the stationary gait. This gait dominates when θ_c is large ($\theta_c > 50°$) or both θ_c and α_s are sufficiently large (shown in the upper right region in the phase diagrams in Figure 1C(iii) and Figure 2C(iii)). In this gait, the link-bot can have a high breathing angle and/or a large flapping range, allowing it to spread wide enough for both side chains to make contact with the wall. This causes the link-bot to push the boundary wall and exhibit very little translational movement.

Overall, link-bot behavior is controlled by the rotational freedom of the bots specified by the link angles. The orientation of individual bots is most strongly controlled by the constraints caused by the overlapping link notches surrounding its crest, rather than through noise or contact with the boundary or other bots. Due to the link structure, these notch angle constraints provide hard rotational limits for each bot that change based on the relative positions of neighboring linked bots. In summary, as the constraints decrease, or as the

values of the angles θ_c, θ_s, and α_s increase, the link-bot gait transitions from translation to oscillation to stationary. It is worth noting that since individual bots are self-propelled along the axis of movement set by their leg tilt direction, the rotational freedom of individual side bots influences the torque they exert on the center bot. This rotational freedom is controlled by θ_s and influenced by neighbor bot positions and thus is incorporated in the link-bot flexibility assessment.

5. Influence of L, d, and N on gait

We investigated the extent to which the gaits are influenced by the link length, bot diameter, and the number of bots, since these are expected to have an effect on the bot dynamics and the torque around the center bot, and thus the resulting gaits. For all link lengths ($1.6 \leq L \leq 6.4$ cm) and bot diameters ($0.3 \leq d \leq 1.5$ cm) tested, the three gaits are present and follow the same link angle relationships as described previously. However, the dynamics of how the side chains apply torque in the three gaits can change slightly. An increased L/d ratio, obtained through increasing the link length or decreasing the bot diameter, seems to make link-bot movement less stable within the translation and stationary gaits, particularly at the gait phase boundaries. In the oscillation gait, the frequency of flips at the wall decreases as L increases due to the increased distance these side bots need to travel to achieve the same flapping angle ranges. In the same way, the flipping frequency decreases as the size of the bots d decreases. These oscillation trends are shown together in Fig. S5, using a shared x axis of L/d.

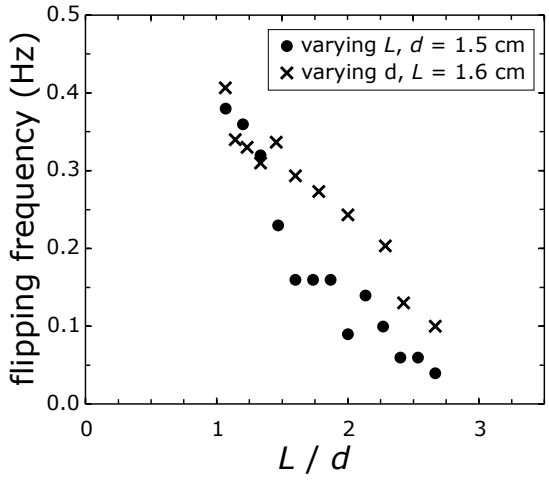

Fig. S5. **Effect of link length L and bot diameter d on oscillation frequency.** Results from simulated link-bots in the oscillation gait showing how the frequency of flips, measured in number of flips per second, changes as a function of the link length and bot diameter. These results are for a link-bot with $N = 7, \theta_c = 60°, \theta_s = 40°, \alpha_s = 30°$, where L and d are varied independently. Within a link-bot, all links and bots have the same L and d values, respectively.

The number of bots N does not significantly effect the movement behaviors of the link-bot. Fig. S6(A-D) show experimental examples of link-bots with $N = 15$ showing the same

translation and oscillation gaits as seen in smaller link-bots, as well as movement between gaits at angle values corresponding to a gait transition point. The corresponding speed profiles are shown in Fig. S6(E and F), alongside simulation results from link-bots with up to 33 bots, showing that the behaviors remain consistent even for very large link-bots. The dynamics of link-bots with different N values in experiment and simulation are shown in Video S2.

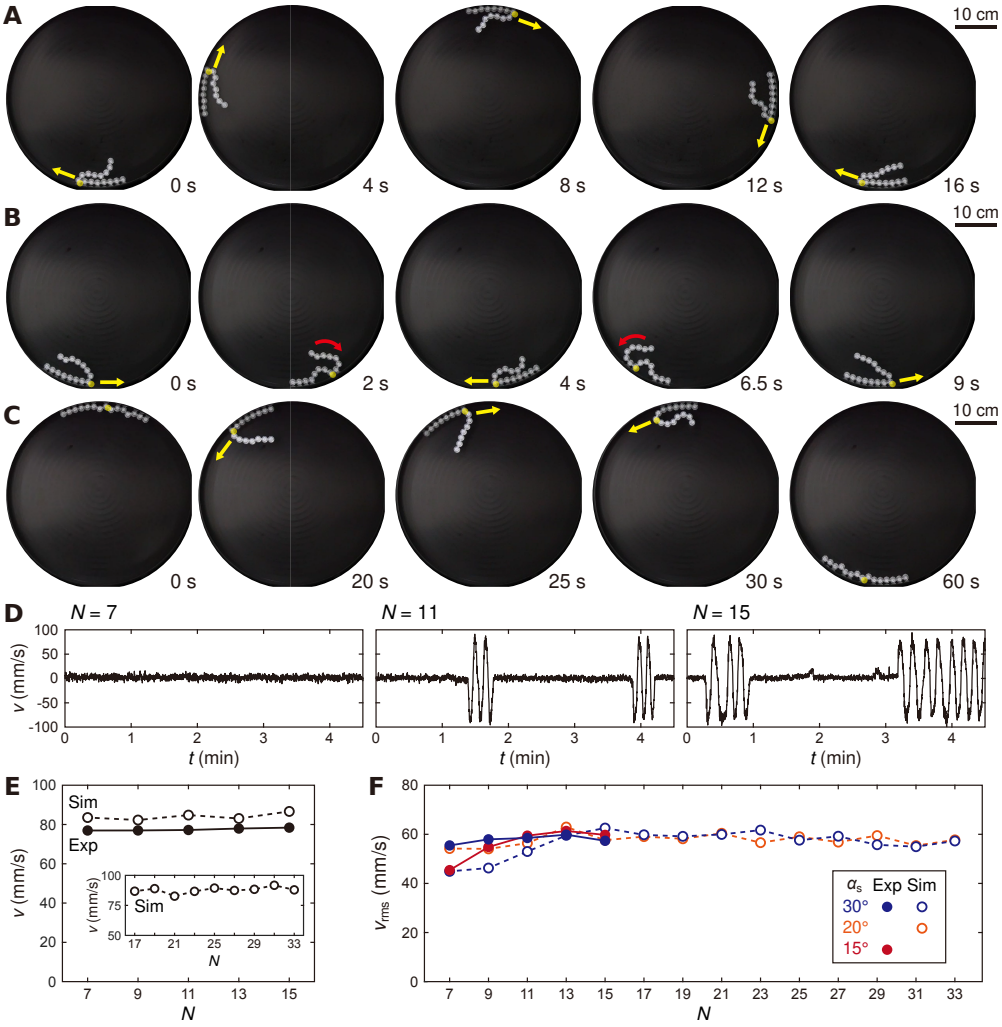

Fig. S6. **Effect of number of bots N on link-bot dynamics.** **(A)** A link-bot with $N = 15$, $\theta_c = 20°$, $\theta_s = 60°$, $\alpha_s = 15°$ exhibits the translation gait, with unidirectional movement along the boundary. **(B)** A link-bot with $N = 15$, $\theta_c = 40°$, $\theta_s = 60°$, $\alpha_s = 30°$ exhibits the oscillation gait, changing direction periodically while moving along the wall. **(C)** A link-bot with $N = 15$, $\theta_c = 40°$, $\theta_s = 60°$, $\alpha_s = 45°$ switches between the stationary gait to the oscillation gait and back again to stationary. The yellow circles indicate the center bot of each link-bot in (A)-(C). **(D)** Velocities at the wall for three link-bots with different number of bots N under the same link angle values as in (C). **(E)** Average speed of a link-bot with respect to N, under the same conditions as in (A), with simulation results up to $N = 33$. **(F)** The relationship of v_{rms} to N while maintaining the same θ_c and θ_s values as in (B) for experiments and simulations. All results are from experiments unless noted otherwise in (E) and (F).

6. Side chain flexibility

The side link angles θ_s and α_s serve to restrict the rotational and translational freedom of the side bots. This directly affects the flexibility of the side chain and controls the resulting flapping movement of the link-bot. Fig. S7 shows the gait phase diagram of a link-bot as a function of these side link angles with respect to θ_c. It can be seen that the center link notch angle θ_c strongly controls the gait, with both side link angles contributing in similar ways: for all but the smallest side link angles, the link-bot transitions from translation to oscillation to stationary gait as θ_c increases. This indicates that θ_s and α_s are microscopic properties that have similar effects on the macroscopic behaviors of the link-bot. Since we are interested in the link-bot behavior at the scale of the gait phenotypes, we take a coarse-grained approach and treat these angles as having similar effects.

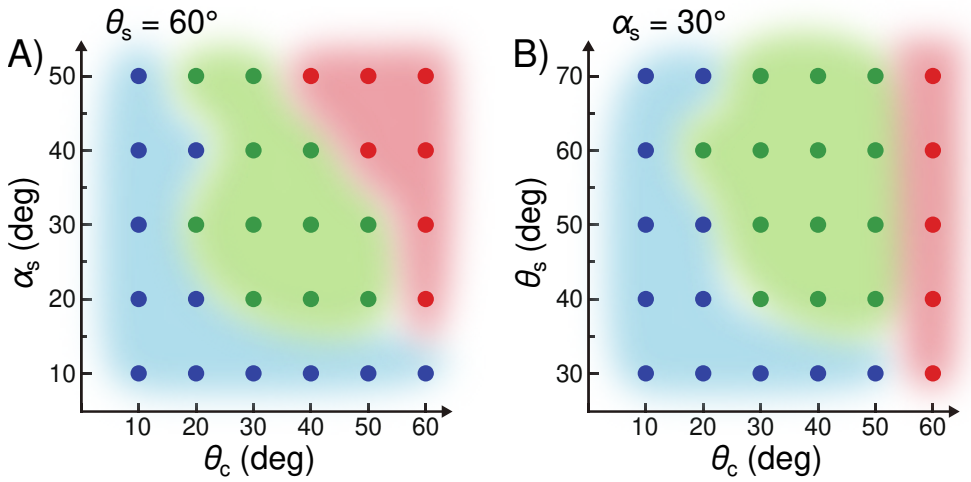

Fig. S7. **Link-bot gait phase diagrams for side link angles.** Phase diagrams showing how the three link-bot gaits are influenced by the side link angles, (**A**) α_s and (**B**) θ_s, obtained from simulations. The translational gait is colored blue, the oscillatory gait is green, and the stationary gait is red.

Upon evaluating the results from a wide range of values, it can be seen that knowing the flexibility of the side chain (defined here as $\theta_s + \alpha_s$) and center notch angle (θ_c) of a link-bot is sufficient to predict its gait. Fig. S8 shows the average distance traveled by the link-bot between flips, which is another way to express the gait type, as a function of the flexibility of the side chain for three representative values of θ_c. As seen in the previous phase diagrams (Fig. S7), θ_c most strongly controls the gait and when this angle is high (ex.

$\theta_c = 60°$, colored purple), the link-bot possesses only the stationary gait. However, for a wide range of low and intermediate θ_c values, the link-bot flexibility predicts the gait. At low θ_c values (e.g. $\theta_c = 10°$, colored yellow), the link-bot trends linearly downwards from translation to oscillation to stationary gaits as its flexibility increases. For intermediate values of θ_c (ex. $\theta_c = 40°$, colored black), this curve takes a sharp reverse sigmoid shape, where the translation and stationary gaits are stable states, with a rapid transition between the two at a constant flexibility value of $\theta_s + \alpha_s \approx 75°$.

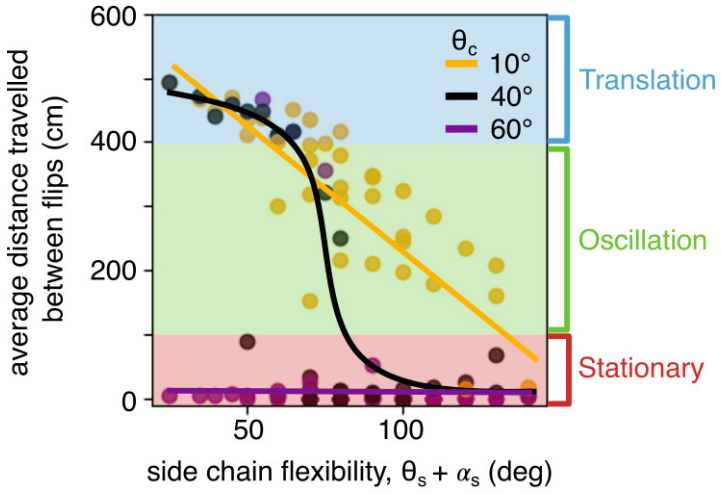

Fig. S8. **Link-bot gait transitions as a function of flexibility.** The average distance traveled by a 7-bot link-bot between flips is given as a function of side chain flexibility for simulated link-bots at three θ_c values. The gait dependence on flexibility shows three different forms based on the center notch angle value, and at low and intermediate values of θ_c the flexibility determines the link-bot gait. The three lines are drawn to guide the eye.

7. Navigation around walls

a. Wall with a gap

The folding and spreading of the link-bot caused by the breathing and flapping movements open up possibilities for interesting behaviors when a link-bot is directed towards a narrow gap in a wall. Experimental snapshots showing link-bots with different α_s and N values passing through a gap are given in Fig. S9. In all these cases, the link-bots pass smoothly through the gap, although the time it takes differs. Link-bots with small α_s and large N values tend to pass through a gap more quickly because they exhibit stronger propulsion in the gap direction.

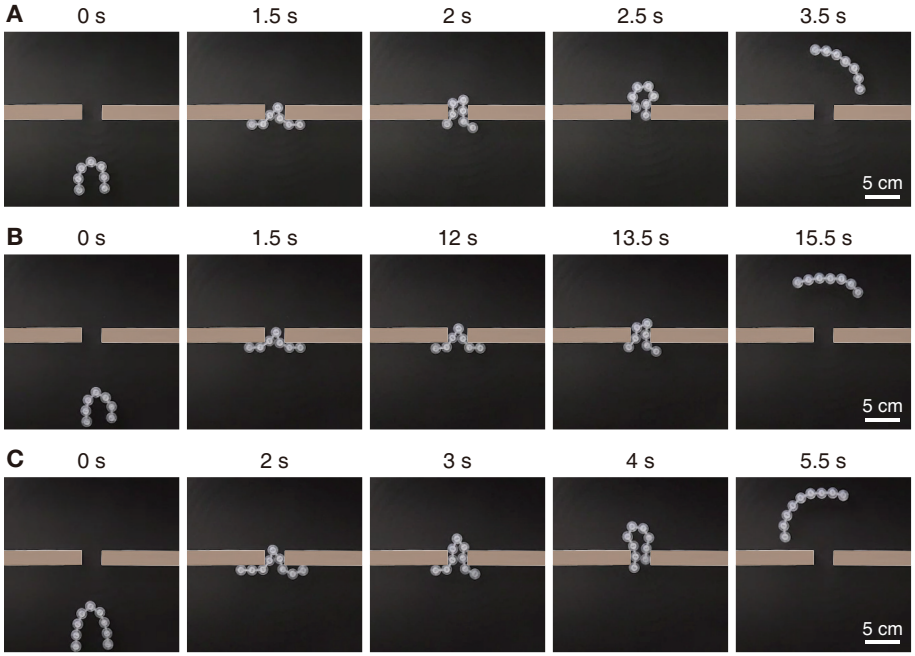

Fig. S9. **Different link-bots passing through a narrow gap.** Link-bots with (**A**) $N = 7$, $\alpha_s = 60°$, (**B**) $N = 7$, $\alpha_s = 75°$, and (**C**) $N = 9$, $\alpha_s = 75°$ exhibit varying passage times to traverse through a gap with a spacing of $2d$. In all experiments, the angle θ_c is fixed at 90°.

Even with large θ_c and α_s values that usually cause the stationary gait at a wall, a link-bot with its center bot aligned with a gap (with spacing $b \geq 2d$) will pass through by folding. This is seen in Fig. S10A and B, which shows the same experimental results as Fig. 3 with more detail. When a link-bot consists of many bots, it can effectively block a gap in a wide range of positions. In experiments, a link-bot biased towards one side of the gap remains

immobile across a large gap up to $b = 3d$ (Fig. S10C). Increasing the size of the gap above this ($b > 3d$), a link-bot will remain in the exploitative state but in this case the side bots will pass through and surround one side of the wall, causing the link-bot to adhere to one edge of the gap and leaving the gap partially open.

The presence of a gap-blocking link-bot provides the opportunity for the selective passage of objects such as other link-bots through the gap. With sufficient contact along the wall, a link-bot can prevent objects approaching from the same side of the wall from passing through the gap (Fig. S10D, also seen in Fig. 4B(i)). However, objects on the opposite side of the link-bot have the potential to pass through the gap by exerting a force against the link-bot that overcomes the link-bot's local propulsion force. This is shown for two examples in Fig S10E and F. Here a longer link-bot (colored gray) blocks a gap and a shorter link-bot (colored pink) approaches from the other side of the wall. The behavior of the blocking link-bot after the passage of the pink link-bot depends on its initial position relative to the gap. When the center of the gap-blocking link-bot is initially near the gap, the pink bots help the central bot squeeze into the gap, causing the entire gray link-bot to pass through the gap and leave the gap open (Fig. S10E). If the central bot is initially distant from the gap, the blocking link-bot will move slightly to the side after letting the pink link-bot pass through the gap, and subsequently closing the gap again (Fig. S10F). This result implies that a considerably long link-bot with its center located far away from the gap will effectively maintain the gap in a closed state for a long time, even in the presence of repeated object passages.

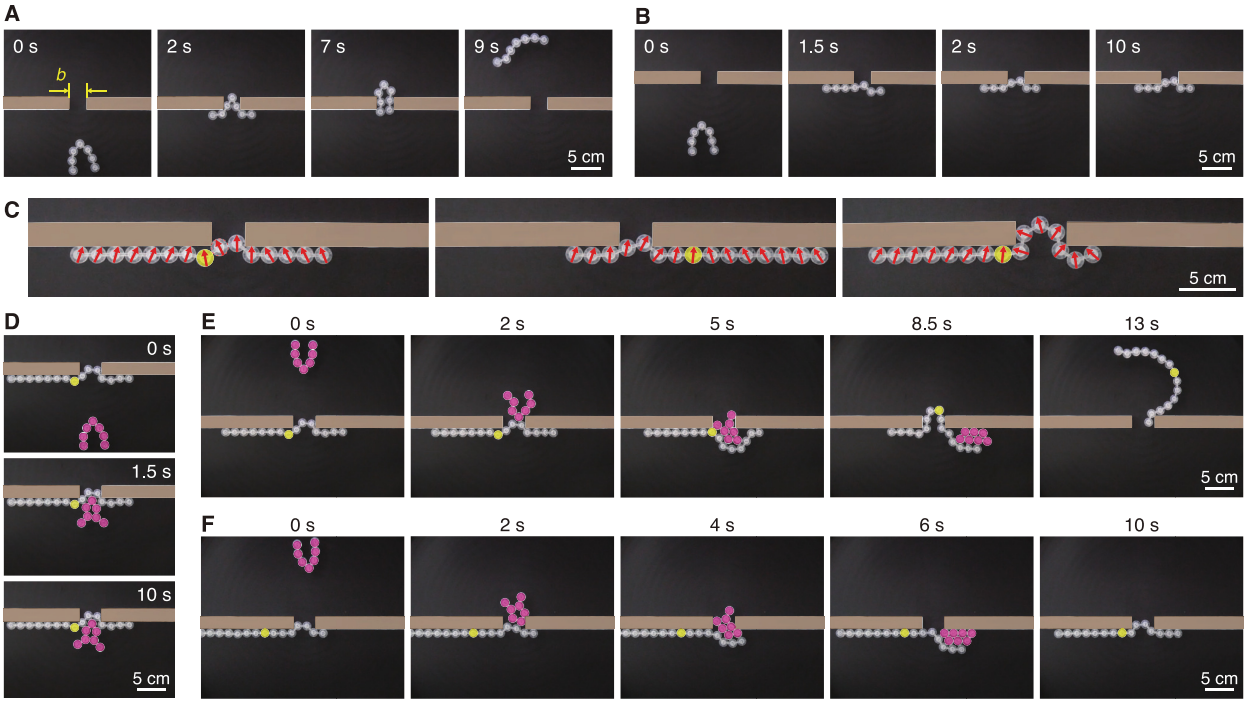

Fig. S10. **Behaviors of a link-bot when encountering a gap in a wall.** (**A** and **B**) A link-bot with $N = 7$ (A) passes through or (B) fails to traverse through a gap of spacing $b = 2d$, depending on the position of the center bot relative to the gap. (**C**) A link-bot with $N = 15$ blocks a gap of $b = 2d$ (left, middle) and a gap of $b = 3d$ (right). The orientation of each bot is indicated by red arrows. (**D**–**F**) A link-bot with $N = 15$ blocks a gap with spacing $b = 2.67d$ and (D) obstructs the same-side transversal motion of a shorter link-bot with $\theta_c = 20°$ and $\alpha_s = 15°$. The blocking link-bot allows the shorter link-bot (marked in pink) to pass through when traveling from the opposite side of the wall. The gap either (E) opens or (F) remains closed depending on the center position of the previously blocking link-bot. All link-bots colored in gray are connected by links with $\theta_c = 90°$ and $\alpha_s = 75°$, and the yellow circles indicate the center bot.

b. Channel

Figures S11A and B show link-bots with $\alpha_s = 15°$ and 75°, respectively, moving through a channel with a spacing of $2d$. Here it is seen that the link-bot with lower flexibility (a smaller α_s) exhibits a higher traveling speed through the channel. This is also shown in Video S3. The speed of link-bots in a narrow channel is plotted in Fig. S11C, showing a decrease with increasing α_s and no significant dependence on N. When compared to the axial speed of a single undisturbed bot ($v_a = 80$ mm/s), link-bots with $\alpha_s = 15°$ and 75° move approximately 25% and 60% slower, respectively, in the channel. This speed reduction occurs due to the rotation of bots towards both walls as α_s increases, leading to a decrease in their propulsion along the length of the channel.

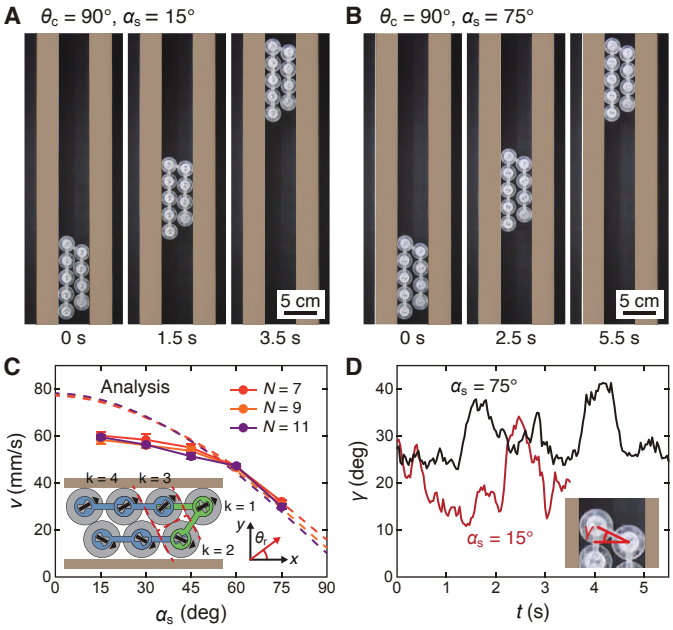

Fig. S11. **Link-bot speed within a narrow channel.** A link-bot with **(A)** $\alpha_s = 15°$ and **(B)** 75° travels in a channel with a spacing of $2d$. (**C**) The average speeds of link-bots with varying N and α_s values when they move through the channel shown in (A) and (B). The dashed lines show the prediction based on the assumption that a link-bot moves with its center angle fully folded and the bots on each side lined up parallel to the wall, as illustrated in the inset image. (**D**) The angle between the line normal to the wall and the line connecting the centers of the two leading bots versus time.

The speed of a link-bot within a channel can be estimated by analyzing the orientation

of each bot. We predict the speed by assuming that the link-bot moves with the bots on each side lined up parallel to the channel wall and the center angle maximally folded, as illustrated in the inset of Fig. S11C. Through geometric analysis, we find the angle θ_{r} which reflects how much each bot has rotated with respect to the direction of link-bot movement as follows:

$$\theta_{\mathrm{r}} = \sin^{-1}\left(\frac{d}{2L}\right), \tag{S1}$$

$$\max\left\{-\frac{\theta_{\mathrm{s}}}{2} - \alpha_{\mathrm{s}}, \sin^{-1}\left(\frac{d}{2L}\right) - \theta_{\mathrm{c}}\right\} \leq \theta_{\mathrm{r}} \leq \min\left\{\frac{\theta_{\mathrm{s}}}{2} - \alpha_{\mathrm{s}}, \sin^{-1}\left(\frac{d}{2L}\right)\right\}, \tag{S2}$$

$$\max\left\{\sin^{-1}\left(\frac{d}{2L}\right), -\frac{\theta_{\mathrm{s}}}{2} + \alpha_{\mathrm{s}}\right\} \leq \theta_{\mathrm{r}} \leq \min\left\{\sin^{-1}\left(\frac{d}{2L}\right) + \theta_{\mathrm{c}}, \frac{\theta_{\mathrm{s}}}{2} + \alpha_{\mathrm{s}}\right\}, \tag{S3}$$

By assuming that the orientation of each bot is centered within its respective angular range, $\theta_{\mathrm{r}} = \theta_{\mathrm{r,ctr}}$, we obtain the estimated speed of the link-bot:

$$v = \frac{v_{\mathrm{a}} \Sigma \cos\theta_{\mathrm{r,ctr}}}{N}. \tag{S4}$$

The speed is depicted by dashed lines in Fig. S11C which shows good agreement with the experimental values (solid lines) for large α_{s}, although a difference between two values is evident as α_{s} decreases. This discrepancy can be attributed to the link-bot's strong propulsion in the travel direction at small α_{s}, which tends to bring adjacent bots closer to side-by-side arrangement with a small angle of γ (Fig. S11D). The consequent jamming leads to substantial resistance and eventually causes the link-bot to move slower than expected.

Although not explored in detail in this work, it is noted that when $\alpha_{\mathrm{s}} > 75$, the side bots are able to rotate such that the link-bot will move in both directions along the channel.

c. Broken parallel walls

When evaluating the link-bot behaviors upon reaching the end of a wall which is adjacent to another parallel one, we only consider link-bot parameters within the translation and oscillation gaits since the stationary gait does not permit exploration. Fig. S12A and B show the same experiments as depicted in Fig. 3C with more detail given, including the angle at contact. When a link-bot reaches the end of a wall along which it was traveling, it will turn slightly towards the wall (due to the center bot moving around the wall corner) and continue in a straight trajectory from the corner of the wall. Upon arriving at a second wall, the movement of the link-bot depends on its gait. A link-bot in the translation gait (shown in Fig. S12A) will continue moving along the second wall in the same direction as it was traveling along the first wall. In contrast, a link-bot in the oscillation gait (shown in Fig. S12B) has more flexible side chains which, facilitated by its arrival at the second wall with a larger incidence angle, causes it to change direction at the wall.

It is important to note that there is some variability across link-bot runs due to the freedom bots have to rotate within their link notches, since θ_{c} and θ_{s} define the limits only. Experiments involving modifications of the distance z between the two walls, shown in Fig. S13, demonstrate that link-bots with $\alpha_{\mathrm{s}} = 30^{\circ}$ change their direction frequently upon encountering a wide gap of $z/d \geq 3$ (with a probability from 69% to 77/%). In contrast, link-bots at a narrow gap ($z/d = 2$) reverse direction less frequently ($\simeq 40\%$) due to obstruction from the original wall. These two behaviors at a series of walls present a bifurcation in the dynamics due to the link-bot gait, which can be controlled by the side chain flexibility through α_{s}. Similar results are obtained if the gait changes by adjusting θ_{c}.

We also evaluated a scenario with a short wall positioned in front of a second wall containing a gap. If a link-bot exhibiting the oscillation gait along the surface approaches the short wall, it can navigate through the obstacle terrain by colliding with the wall in front, circumventing the wall, changing direction at the wall behind, and subsequently passing through the gap, shown in Fig. S12C. This passage is feasible only when the length of the front wall is shorter than s, the distance the link-bot travels between each flip; the link-bot is unable to go around the wall if the length of the wall exceeds s. These observations in both scenarios show the potential of traversing or maneuvering around environmental features depending on the design of the link-bot.

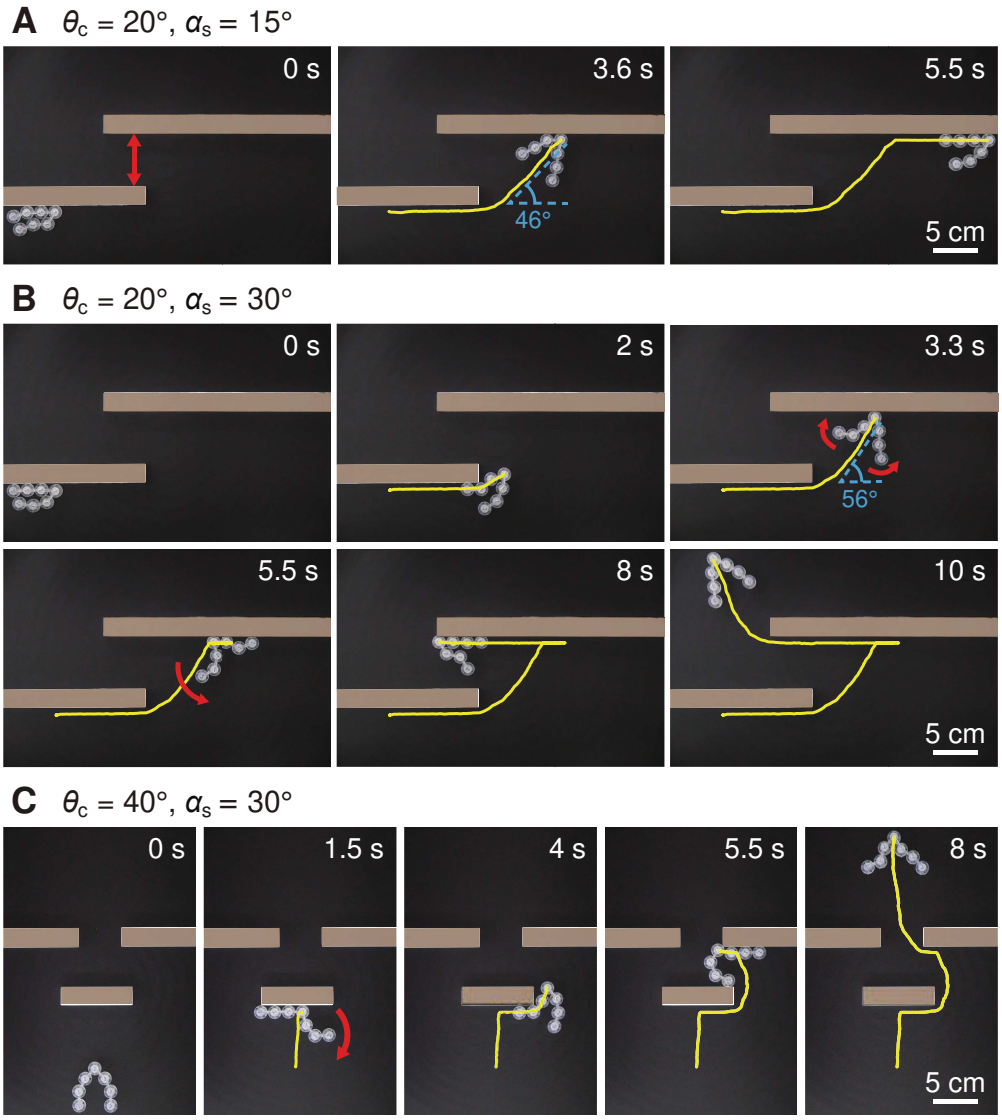

Fig. S12. **Environmentally-adaptive link-bots with adjustable trajectories.** The trajectory of a link-bot consisting of $N = 7$ bots connected by center links with $\theta_c = 20°$ and side links with **(A)** $\alpha_s = 15°$ and **(B)** $30°$ when it reaches the end of a wall and encounters another parallel wall with a distance $z = 4d$ from the original wall. (**C**) The trajectory of a link-bot with $N = 7$, $\theta_c = 40°$, and $\alpha_s = 30°$ when it encounters a short wall positioned $3d$ in front of a wall with a gap.

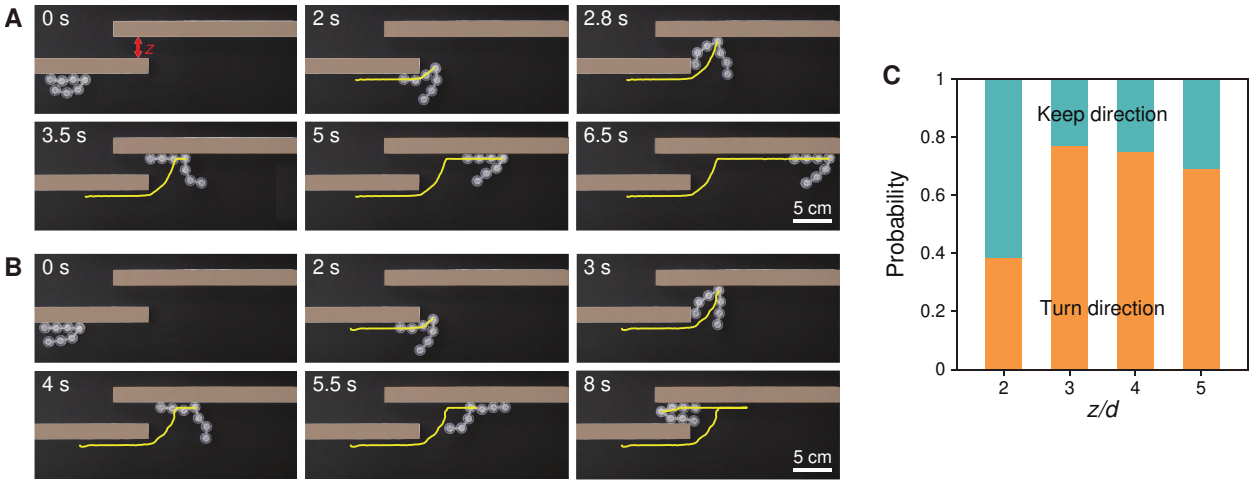

Fig. S13. **Navigation of link-bots in an environment with two parallel walls.** When a link-bot with $N = 7$, $\theta_c = 20°$, $\alpha_s = 30°$ approaches the end of one wall and encounters another parallel wall with a separation distance of $z = 2d$, it **(A)** maintains or **(B)** reverses its direction along the wall. (**C**) Probability for a link-bot to maintain or to reverse its direction as a function of the relative separation between parallel walls, z/d.

d. Curved wall

When a link-bot encounters a sufficiently large stationary curved obstacle, it will move with the same translation and oscillation gaits as seen along a straight wall, shown with experimental snapshots in Fig. S14A and B, and velocity profiles in Fig. S14C. When the obstacle is small, however, the link-bot is likely to deviate from the highly curved surface, as seen in Fig. S14D. These behaviors are also shown in Video S3. By creating an asymmetry in the link-bot, this surface-leaving behavior can be avoided. This is shown in Fig. S14E and F, where single inverted side link causes the link-bot to travel along a highly curved surface without leaving. Therefore, the path along or away from a curved surface can be adjusted by the link-bot link properties and surface curvature. One possible function of this property is to selectively sort link-bots, as shown in Fig. S15 (which displays the results from Fig. 3D in more detail)

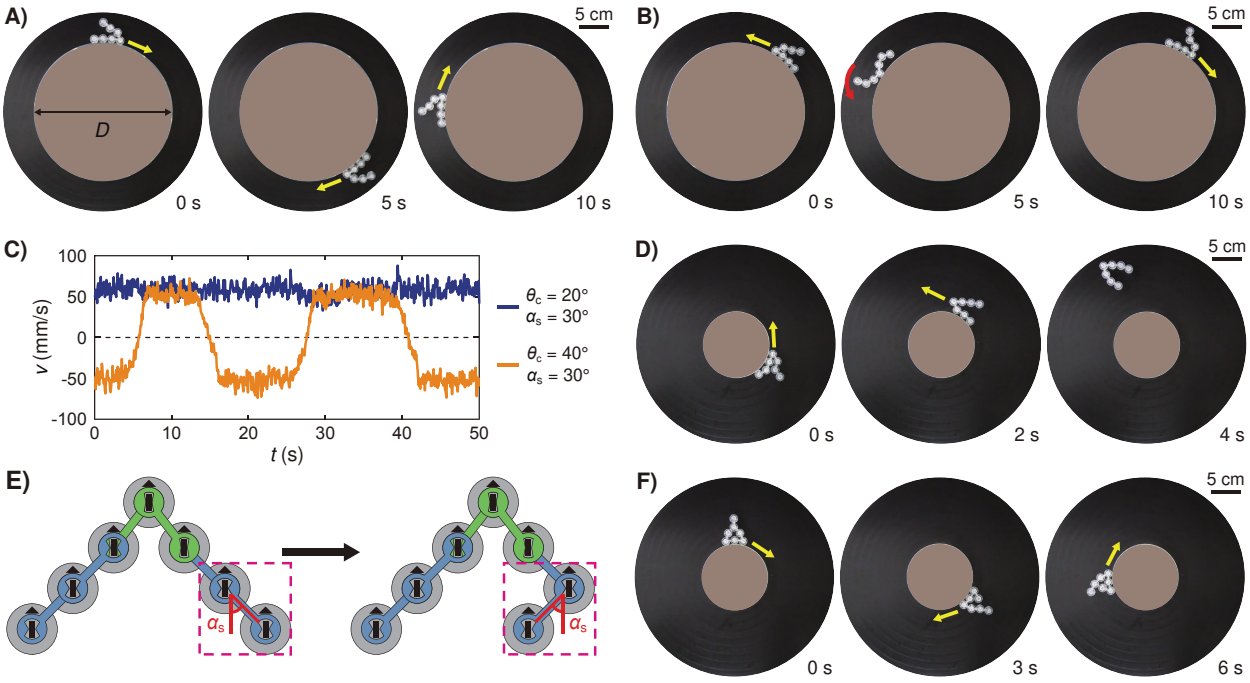

Fig. S14. **Behaviors of a link-bot encountering a circular stationary object.** A link-bot with **(A)** $\theta_c = 20°$, $\alpha_s = 30°$ and **(B)** $\theta_c = 40°$, $\alpha_s = 30°$ moving along an object with diameter $D/d = 16.7$, and **(C)** the corresponding velocities of the link-bots as a function of time. **(D)** A link-bot with $\theta_c = 20°$, $\alpha_s = 30°$, moving around and then away from an object with $D/d = 8$. **(E)** Schematic of an asymmetric link-bot with a folded right end due to an inverted side link. **(F)** A link-bot with $\theta_c = 20°$, $\alpha_s = 45°$, and folded at right end, moving along an object with $D/d = 8$.

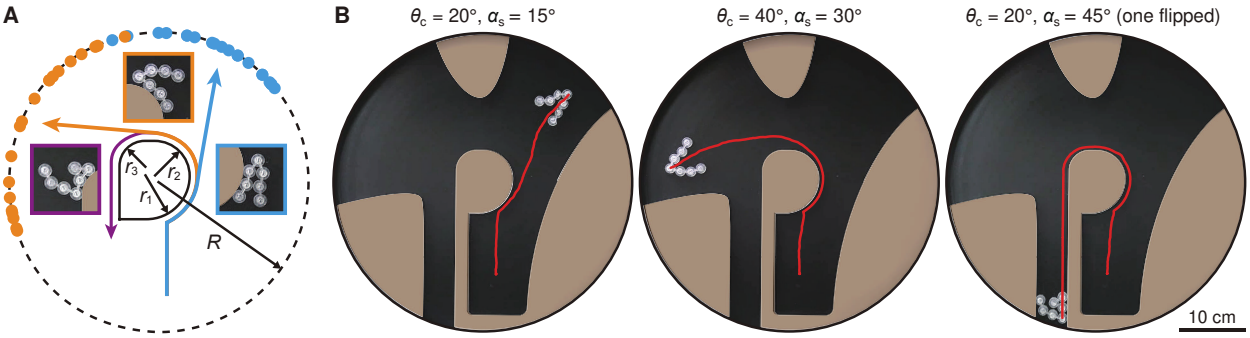

Fig. S15. **Selective sorting of link-bots through an obstacle with multiple curvatures** (**A**) The positions of the center bot of the link-bots upon reaching a distance of $R/d = 12$ from the center of an obstacle after encountering the obstacle with varying radius of curvature, $r_1/d = 3.5$, $r_2/d = 2.8$, $r_1/d = 2$. Inset images show link-bots with $\theta_c = 20°$, $\alpha_s = 15°$ (blue), $\theta_c = 40°$, $\alpha_s = 30°$ (orange), and $\theta_c = 20°$, $\alpha_s = 45°$ with a flipped link at the left end (purple). (**B**) Separation of the three types of link-bots into target compartments through collisions with the obstacle shown in (A). The red lines show the trajectories traveled by the center bot of each link-bot.

8. Link-bot transporting mobile object

link-bots exhibit diverse transportation behaviors when interacting with a mobile object. Varying the link-bot geometric parameters causes five distinct behaviors: carrying the object forwards or backwards, moving forwards or backwards away from the object, and stasis while in contact with the object. These transportation behaviors are shown for experiments in Fig. S16. These movement modes are dependent on the relative geometries of the link-bot and object, shown in phase diagrams of D/d vs N. Fig. S17 shows phase diagrams of the link-bot transportation behaviors for three α_{s} values: 75°, 60°, and 45°. In all three cases, link-bots carry the object forward in the upper left region (shorter link-bot and larger object), with the corresponding green regime expanding as α_{s} increases. Conversely, moving towards the right region (longer link-bot), link-bots are more likely to move forward away from the object, resulting in the widening of the blue regime as α_{s} decreases. Link-bots have a higher probability of moving backward in the lower right region, with only link-bots having large α_{s} capable of carrying the object backward. Bicolored circles in all panels represent the conditions under which either behavior can occur. In these cases, link-bots colliding with the object at a slight angle can unfold asymmetrically, thereby increasing the probability of moving forward away from the object.

To gain a quantitative understanding of how each transport regime in these phase diagrams appears, we analyse the orientation of each bot when the link-bot establishes conformal contact with the object, as shown in Fig. S17B. Through geometric analysis, we obtain the range of angle θ_{r} by which the n^{th} bot from the center has rotated with respect to the orientation of the center bot as follows:

$$\begin{aligned} \max\left\{\frac{\pi+3\beta-\theta_{\mathrm{s}}-2\alpha_{\mathrm{s}}}{2}, \frac{\pi+\beta-2\alpha-2\theta_{\mathrm{c}}}{2}\right\} \leq \theta_{\mathrm{r}} \leq \\ \min\left\{\frac{\pi+3\beta+\theta_{\mathrm{s}}-2\alpha_{\mathrm{s}}}{2}, \frac{\pi+\beta-2\alpha}{2}\right\} \quad (n=1)\,, \end{aligned} \tag{S5}$$

$$\frac{\pi+(2n+1)\beta-\theta_{\mathrm{s}}-2\alpha_{\mathrm{s}}}{2} \leq \theta_{\mathrm{r}} \leq \frac{\pi+(2n-1)\beta+\theta_{\mathrm{s}}-2\alpha_{\mathrm{s}}}{2} \quad \left(1<n<\frac{N-1}{2}\right), \tag{S6}$$

$$\frac{\pi+(N-2)\beta-\theta_{\mathrm{s}}-2\alpha_{\mathrm{s}}}{2} \leq \theta_{\mathrm{r}} \leq \frac{\pi+(N-2)\beta+\theta_{\mathrm{s}}-2\alpha_{\mathrm{s}}}{2} \quad \left(n=\frac{N-1}{2}\right), \tag{S7}$$

where $\beta = 2\sin^{-1}[L/(D_{\mathrm{obj}}+d)]$ is the angle formed by the two lines connecting the center of the object and the centers of adjacent bots. By assuming $\theta_{\mathrm{r}} = \theta_{\mathrm{r,ctr}}$, we calculate the

normalized momentum of the link-bot:

$$\frac{P}{mv} = \Sigma \cos \theta_{\mathrm{r,ctr}}, \tag{S8}$$

for link-bots not long enough to encircle the object. The result is shown in Fig. S17C, where the colored regions correspond to the transport regimes represented by the same colors in Fig. S17A. When the link-bot curvature upon enclosing an object (looking at the θ_{r} value) is low, it will exhibit greater forward momentum. Consequently, the larger the object, the greater the link-bot length at which the forward momentum starts to decrease. The similarity of transport regime boundaries in Fig. S17A and C implies that $\frac{P}{(mv)}$ can approximate the physical effects of $\frac{D_{\mathrm{obj}}}{d}$.

Increasing the number of bots N within the link-bot causes a decrease in momentum, which implies that these additional side bots provide propulsion force in the backward direction. This trend is seen when the link-bot retracts away from the object and subsequently moves past it (boundary of blue shaded region in Fig. S17 phase diagrams). More significant backwards movement is seen when the link-bot encloses the object and carries it backward (high α_{s} values, red shaded region) and when the link-bot separates from the object and retreats backwards (low α_{s} values, orange shaded region). The inset images in Fig. S17C show examples when link-bots alter their shape as both side chains retract backwards, eventually moving in the opposite direction compared to when they were in full conformal contact with the object.

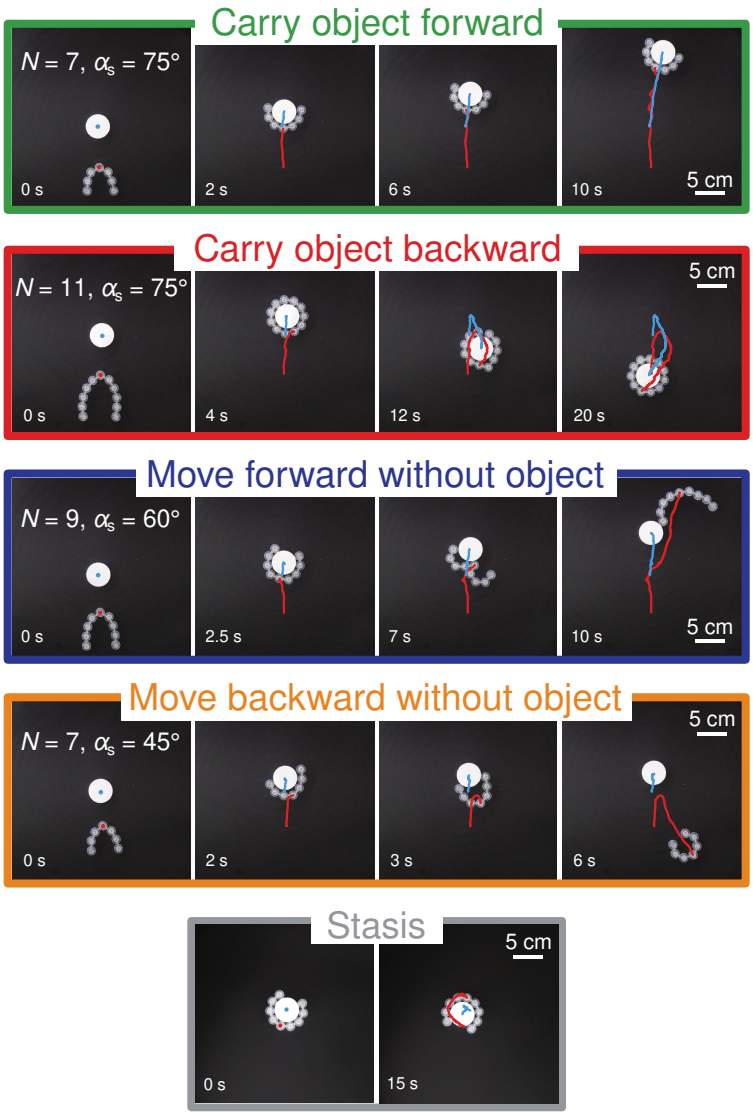

Fig. S16. **Link-bots perform selective transportation**. By adjusting the link angular constraints and number of bots within a link-bot, its transport behaviors can be controlled. Snapshots show the following behaviors of the link-bot in experiments when it encounters a passive mobile object: pushing the object forwards (green border), pulling the object backwards (red border), passing forwards without carrying the object (blue border), moving backwards away from the object without carrying it (orange border), and wrapping around the object and remaining stationary (gray border). The link-bot trajectories are shown in red, the object trajectories are blue.

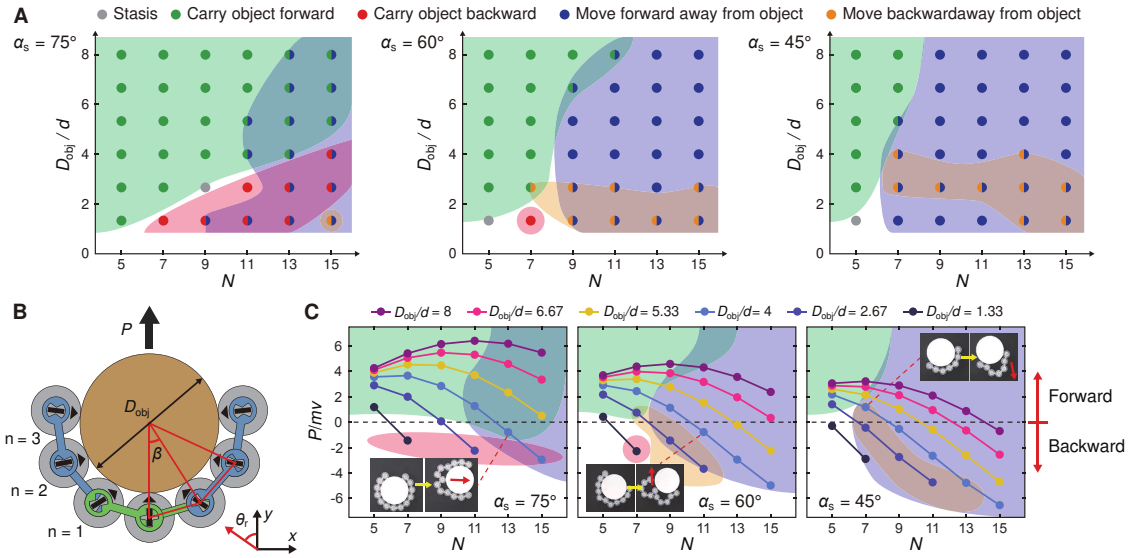

Fig. S17. **Phase diagrams showing link-bot transportation behaviors with respect to object and link-bot sizes.** (**A**) Link-bot behaviors after colliding with an unanchored object as N and D are varied across three α_s values. (**B**) Schematic depicting a link-bot in conformal contact with an object, displaying momentum P. (**C**) Normalized momentum of the link-bot while in conformal contact with the object under each condition. The colored areas correspond to the same colored regimes shown in (A). The inset images show link-bots losing conformal contact and eventually moving in the opposite direction to the calculated momentum. The angle θ_c is fixed at 90° in (A–C).

9. Link-bots interacting with objects of various shapes

The versatility provided by the threshold link angle constraints allows link-bots to enclose a variety of shapes, not limited to circles. Fig. S18 shows snapshots of experimental link-bots surrounding and enclosing an ellipse, square, triangle, L-shape, and cross shape object. A corresponding video is in Video S3.

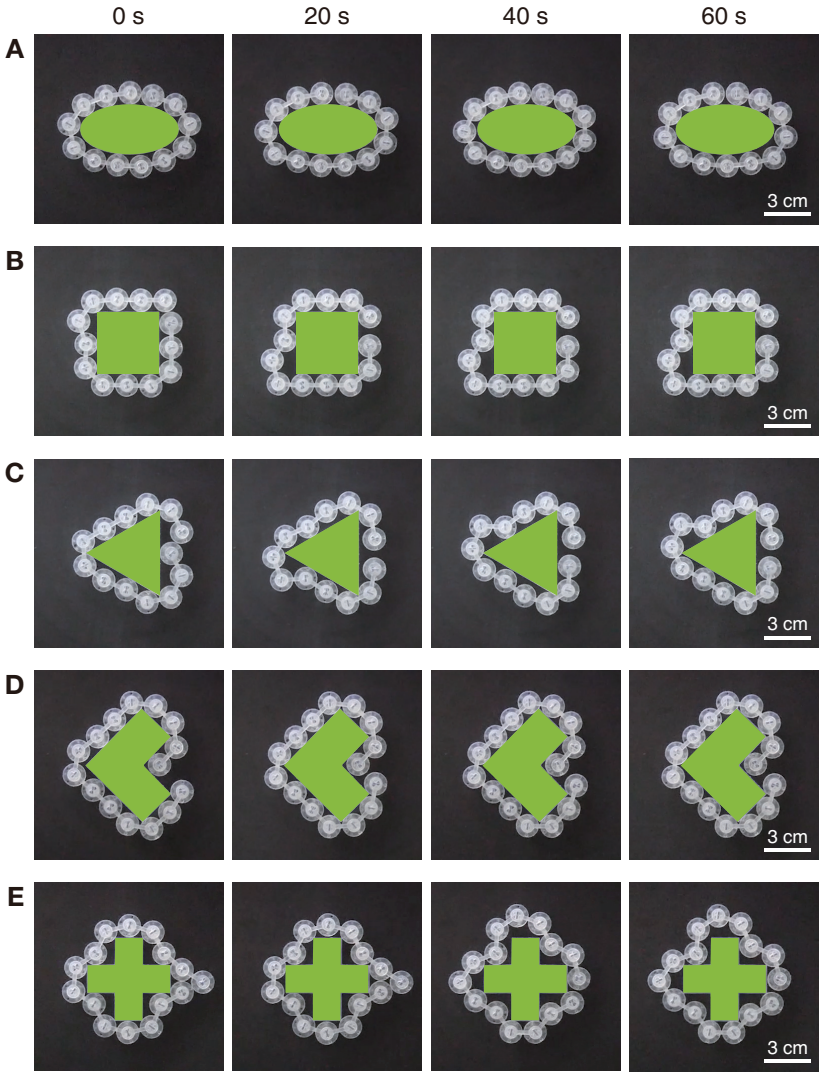

Fig. S18. **Link-bots enclosing objects of different shapes.** (**A**) Ellipse, (**B**) Square, (**C**) Triangle, (**D**) L- shape, (**E**) Cross shape. In all experiments, the angles θ_c and α_s are set to 90° and 75°, respectively.

10. Link-bots in multi-component environments

The link-bot may not always exhibit the same behavior under identical conditions due to the threshold nature of the angle constraints. However, through connecting the link angle parameters to gaits and other behaviors we see that the link-bot has stochastically predictable functions in a given environment. Examples of one or more link-bots interacting with complex environments consisting of walls and obstacles are given in Fig. S19 and Video S4.

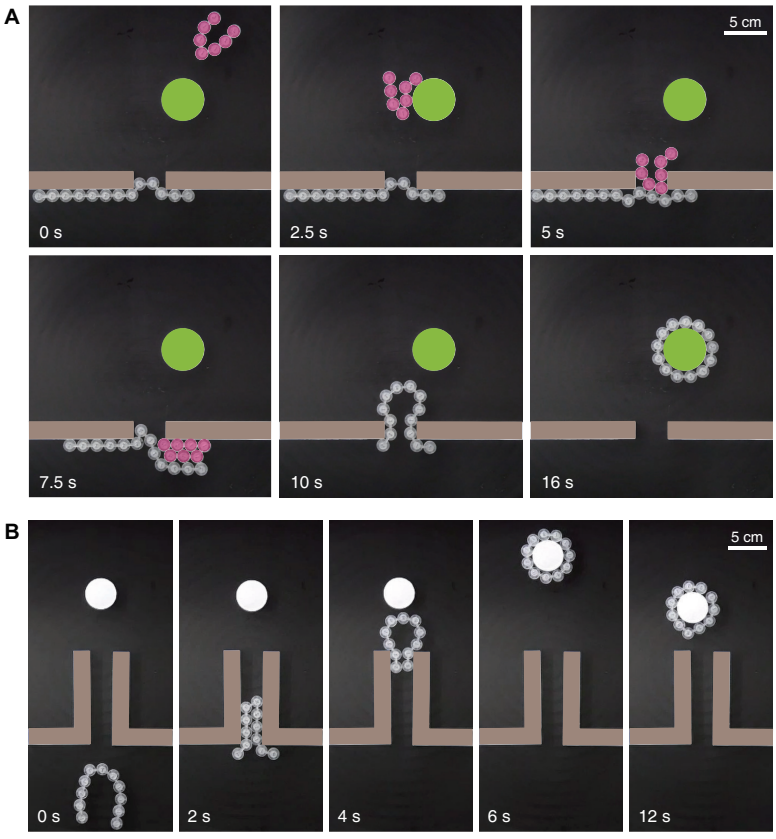

Fig. S19. **Link-bots locomoting, navigating, transporting, and interacting in multi-component environments.** (**A**) A link-bot with $N = 13$, initially blocking a narrow gap, allows a short link-bot (which has just traveled around an object) to pass through, and then the long link-bot itself passes through the gap to wrap around the fixed circular object. (**B**) A link-bot with $N = 11$ crosses a narrow channel, fully encloses an unfixed circular object, and subsequently transports it backward.

11. Video captions

The dynamics of link-bots in simulations and experiments are shown in Video S1–5.

Video S1. Locomotion: Link-bot movement with and without walls present, showing effect of link angles and the resulting link-bot gaits. Examples from experiments and simulations of link-bots exhibiting directed locomotion without any wall interactions as well as when encountering a wall. Changing the center and side link angles changes the collective behavior of the link-bot at a wall, and examples here systematically vary the link angles to show their effects on the link-bot gait. Parameters not listed in the video itself are provided in Table I.

Video S2: Behaviors of link-bots with different number of bots N. Experimental and computational results showing the link-bot gaits at a wall when the number of bots are varied. Four different link angles are shown to include the translation, oscillation, and stationary link-bot gaits. The parameters not listed in the video are provided in Table I.

Video S3: Navigation and Interactions: Experimental videos for link-bot movement at broken parallel walls, at a gap in a wall, and with an object. The navigation of link-bots across parallel walls and through gaps in walls depends on their link angle parameters, which is shown for 9 different examples. Interactions between two link-bots can cause both to become stuck at a gap in a wall (competitive interaction) or to aid one or both to pass through the gap (cooperative interactions). Cooperative and competitive interactions with a dumbbell-shaped object are dependent on the number of bots within each link-bot. All videos are at 1x speed and parameters not given in the video frames are listed in Table I.

Video S4: Navigation and Transportation: Experiments and simulations showing link-bot dynamics within a channel and at a curved wall, as well as link-bots engaged in selective transportation of objects. The speed and direction of link-bots as they navigate a narrow channel or curved walls depend on the link-bot center and side link angles. An experimental video shows that link-bots have the ability to self-sort according to their link angles when interacting with a curved wall. The dynamics of link-bots engaging in selective transportation of loads are shown in experiments and computations,

matching the images shown in Fig. 4 and Fig. S16. Examples of experimental link-bots enclosing non-circular objects are also given. All videos are at 1x speed unless specified otherwise and parameters not given in the video frames are listed in Table I.

Video S5: Link-bots performing sequential functional behaviors in multicomponent environments. Experimental videos showing link-bot dynamics within three environments, each containing multiple features such as walls (straight and curved; with and without gaps), channels, and fixed or movable objects. In each case, the link-bots show that their navigation and interaction with surfaces, objects, and other link-bots can be controlled by adjusting their link angles. Link-bot parameters not given in the video are provided in Table I.